TECNOLOGIA BARREIRO
ESCOLA SUPERIOR
POLITÉCNICO SETÚBAL

ÉRICA
ALEXANDRA
ANDRÉ
SALVADOR

BIODIESEL PRODUCTION BY OLEIC ACID METHANOLYSIS OVER WASTE BIOMASS HYDROCHAR CATALYSTS

Thesis to obtain the Master's Degree in Biological and Chemical Engineering

SUPERVISORS

Doctor Ana Paula Vieira Soares Pereira Dias

Doctor Maria de Fátima Nunes Serralha

September 2024

ÉRICA
ALEXANDRA
ANDRÉ
SALVADOR

BIODIESEL PRODUCTION BY OLEIC ACID METHANOLYSIS OVER WASTE BIOMASS HYDROCHAR CATALYSTS

BOARD OF EXAMINERS

Chairperson: Doctor Maria de Lurdes de Figueiredo Gameiro, Escola Superior de Tecnologia do Barreiro, Instituto Politécnico de Setúbal

Supervisor: Doctor Ana Paula Vieira Soares Pereira Dias, Instituto Superior Técnico, Universidade de Lisboa

Member of the Board: Doctor Bruna Alexandra Canuto Rijo, Instituto Politécnico de Portalegre

September 2024

AGRADECIMENTOS

À Professora Ana Paula Dias, cuja ajuda foi verdadeiramente fundamental para a concretização deste trabalho. A generosidade ao disponibilizar o laboratório foi apenas uma das muitas formas com que contribuiu para o meu sucesso. Agradeço profundamente pelo tempo incalculável que dedicou ao meu projeto, pela paciência, e pelo conhecimento vasto que partilhou comigo.

À Professora Fátima Serralha, pela orientação cuidadosa e pelas sugestões valiosas que ajudaram a moldar esta tese. Agradeço o tempo e a dedicação com que acompanhou o desenvolvimento do meu trabalho.

Aos meus pais, que sempre fizeram o possível e o impossível para me proporcionar as melhores condições de estudo e de vida. O amor e confiança foram essenciais para que eu pudesse chegar até aqui.

Ao meu namorado, por estar ao meu lado desde o primeiro dia do meu percurso académico. O seu apoio constante, carinho e compreensão tornaram cada etapa mais leve e, nos momentos mais desafiantes, foi e será sempre o meu pilar.

Pedro Santos, parte essencial do “trio maravilha”, esteve ao meu lado em longas noites de estudo e desafios académicos. Admirável pela sua dedicação e espírito resiliente como trabalhador-estudante, mostrou-me o que é possível alcançar com esforço e determinação.

Às amizades formadas no laboratório, Pedro, Francisco, Nawik e Tiago, pelo apoio constante, pelas valiosas partilhas e pelos grandes momentos que tivemos.

RESUMO

Abordar as alterações climáticas requer uma transição dos combustíveis fósseis para fontes de energia renováveis. O biodiesel apresenta-se como uma alternativa promissora ao gasóleo convencional. Para aumentar a sustentabilidade do biodiesel, é crucial utilizar óleos de fritura usados como matéria-prima. A transesterificação ácida oferece um método mais eficiente para o processamento desses óleos em comparação com a catálise básica. Embora os catalisadores ácidos homogéneos, como o ácido sulfúrico, sejam comumente utilizados, a sua natureza corrosiva e os riscos de segurança associados destacam a necessidade de substitutos. Em resposta, surgiram catalisadores ácidos heterogéneos como substitutos viáveis. Este estudo explora a esterificação do ácido oleico com metanol, utilizando catalisadores à base de hidrocarvão derivados de biomassa. Os hidrocarvões foram sintetizados a partir de amido de milho, frutose, sacarose, casca de laranja e casca de banana, através de carbonização com sulfonação simultânea a 150°C sob pressão atmosférica. O processo de carbonização, com a duração de 5 horas, foi realizado utilizando diferentes quantidades de ácido sulfúrico (relação de massa de biomassa entre 1:1 e 3:1) para aumentar a área de superfície e melhorar a grafitização e estabilidade. Os catalisadores preparados, frescos e pós-reação, foram extensivamente caracterizados utilizando difração de raios-X (DRX), Espectroscopia de Infravermelho (ATR-FTIR), análise termogravimétrica (TGA), Microscopia Eletrónica de Varrimento (MEV), e a composição química foi analisada através de espectroscopia de raios-X por dispersão de energia (EDS). O desempenho dos catalisadores foi avaliado durante a esterificação do ácido oleico. Os catalisadores de hidrocarvão comportaram-se de forma diferente, dependendo da sua biomassa de origem, das proporções de sulfonação e das condições de reação. O catalisador à base de amido de milho alcançou um rendimento notável de 76,4% de MO com uma relação molar de sulfonação de 1:5. Por outro lado, o catalisador derivado de sacarose apresentou o maior rendimento de MO, com 90,1% numa relação molar de 1:1, embora o rendimento tenha diminuído ligeiramente à medida que a proporção de sulfonação aumentava. Curiosamente, o hidrocarvão derivado de casca de banana mostrou um rendimento ótimo de MO de 53,1% com uma relação de sulfonação de 3:1, diminuindo com a hidrólise; para o hidrocarvão de casca de laranja, o maior rendimento foi de 87,8%, demonstrando um comportamento distinto influenciado pela sua estrutura e pelo processo de sulfonação, quase não alterando os resultados do hidrocarvão derivado de sacarose. O efeito do teor de ácido oleico e de água foi avaliado, confirmando os seus efeitos prejudiciais. Este trabalho de tese foca-se na esterificação do ácido oleico com metanol, utilizando vários catalisadores de hidrocarvão derivados de resíduos agrícolas e alimentares. O principal objetivo foi otimizar as condições de reação para alcançar altos rendimentos de oleato de metilo, promovendo simultaneamente uma produção de biodiesel sustentável e económica. O desenho experimental empregou uma relação molar de 12:1 de metanol para ácido oleico, com uma temperatura de reação consistente de 67°C para o refluxo total de metanol, garantindo o ambiente de reação adequado.

PALAVRAS-CHAVE: Hidrocarvão, esterificação, oleato de metilo, biodiesel, catalisadores.

ABSTRACT

Addressing climate change requires a shift from fossil fuels to renewable energy sources. Biodiesel presents a promising alternative to conventional diesel fuel. To enhance the sustainability of biodiesel, it is crucial to utilize waste frying oils as a feedstock. Acid transesterification offers a more efficient method for processing these oils compared to base catalysis. Although homogeneous acid catalysts, such as sulfuric acid, are commonly used, their corrosive nature and associated safety risks highlight the need for replacements. In response, heterogeneous acid catalysts have emerged as viable replacements. This study explores the esterification of oleic acid with methanol using biomass-derived hydrochar-based catalysts. Hydrochars were synthesized from corn starch, fructose, sucrose, orange peel, and banana peel through carbonization with simultaneous sulfonation at 150°C under atmospheric pressure. The carbonization process, lasting 5 hours, was performed using different amounts of sulfuric acid (biomass mass ratio between 1:1 and 3:1) to increase surface area and improve graphitization and stability. The prepared catalysts, fresh and post-reaction were extensively characterized using X-ray diffraction (XRD), Infrared Spectroscopy (ATR-FTIR), thermogravimetric analysis (TGA), Scanning Electron Microscopy (SEM) and the chemical composition was analyzed using energy-dispersive X-ray spectroscopy (EDS). The catalysts performances were evaluated during the oleic acid esterification. The hydrochar catalysts behaved differently depending on their biomass feedstock, sulfonation ratios, and reaction conditions. The cornstarch-based hydrochar catalyst achieved a notable yield of 76.4% MO at a 1:5 molar sulfonation ratio. On the other hand, the catalyst from sucrose exhibited the highest MO yield of 90.1% at a 1:1 molar ratio, though the yield slightly declined as the sulfonation ratio increased. Interestingly, the banana peel-derived hydrochar shown an optimal MO yield of 53.1% at a 3:1 sulfonation ratio and decreased as hydrolysis for orange peel hydrochar, the highest yield was 87.8%, demonstrating a distinct behavior influenced by its structure and the sulfonation process, almost not changing the results of the sucrose-based hydrochar. The effect of oleic and water content was evaluated, confirming its hindering effects. This thesis work focuses on the esterification of oleic acid with methanol using various hydrochar catalysts derived from agricultural and food wastes. The primary objective was to optimize the reaction conditions to achieve high methyl oleate yields while promoting sustainable and cost-effective biodiesel production. The experimental design employed a 12:1 molar ratio of methanol to oleic acid, with a consistent reaction temperature of 67°C for methanol total reflux, ensuring the appropriate reaction environment.

KEYWORDS: hydrochar, esterification, methyl oleate, biodiesel, catalysts.

TABLE OF CONTENTS

List of Figures

List of Tables

Acronyms

ASTM - American Society for Testing and Materials
ATR - Attenuated Total Reflectance
BP - Banana Peel
Bxx - Biodiesel Blends (e.g., B100, B7)
CH - Carbohydrates
EDS - Energy Dispersive Spectroscopy
FAME - Fatty Acid Methyl Esters
FFA - Free Fatty Acids
FTIR - Fourier Transform Infrared Spectroscopy
HC - Hydrochar
HTC - Hydrothermal Carbonization
HTG - Hydrothermal Gasification
HTL - Hydrothermal Liquefaction
ICDD - International Centre for Diffraction Data
ISO - International Organization for Standardization
MO - Methyl Oleate
MPa - Megapascal (Pressure Unit)
NaOH - Sodium Hydroxide
OA - Oleic Acid
OP - Orange Peel
PRC - Post Reaction Catalyst
RPM - Revolutions Per Minute
SEM - Scanning Electron Microscopy
SEM-EDS - Scanning Electron Microscopy with Energy Dispersive Spectroscopy
SCA – Short Chain Alcohol
TGA - Thermogravimetric Analysis
XRD - X-ray Diffraction

1. INTRODUCTION

1.1. SCOPE AND MOTIVATION

Over the last few years, climate change has had a major impact due to the quantities of carbon dioxide (CO_2) emitted into the atmosphere, with this being due to the excessive burning of fossil fuels for the production of electricity, heat, and for the use in transport [1]. With the continued use of fossil fuels, carbon dioxide is the main abundant anthropogenic gas, which can remain in the atmosphere for thousands of years [2]. Figure 1 shows the increase in CO_2 emissions over the years, highlighting that in 2023, 35.8 Gt of carbon dioxide was generated by the combustion of energy and industrial processes, and Figure 2, shows the main sectors responsible for the increase in these emissions between 1970 and 2023.

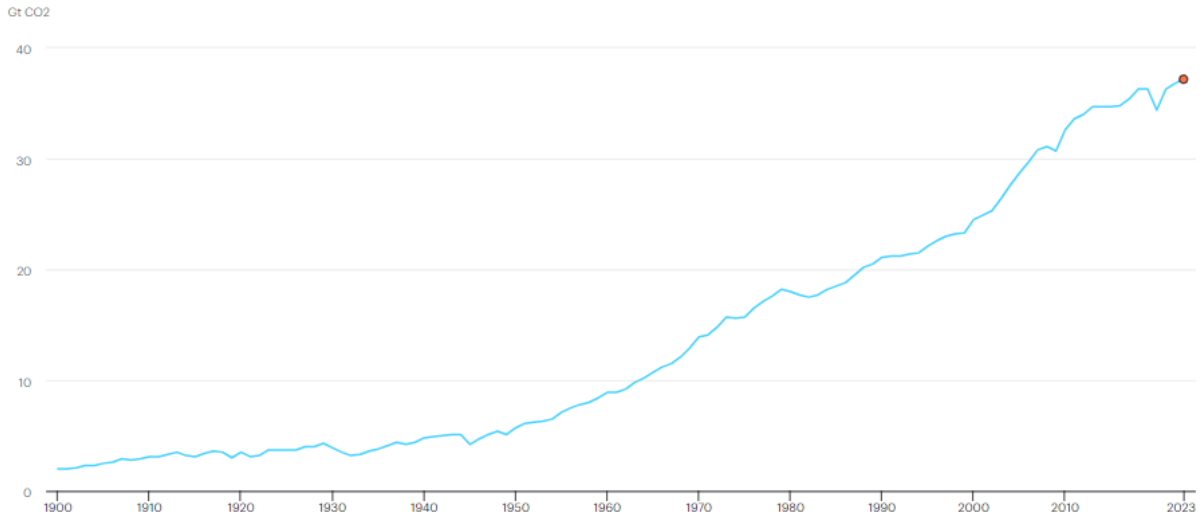

Figure 1 - Evolution of the CO_2 emissions over the last decade (adapted from [3])

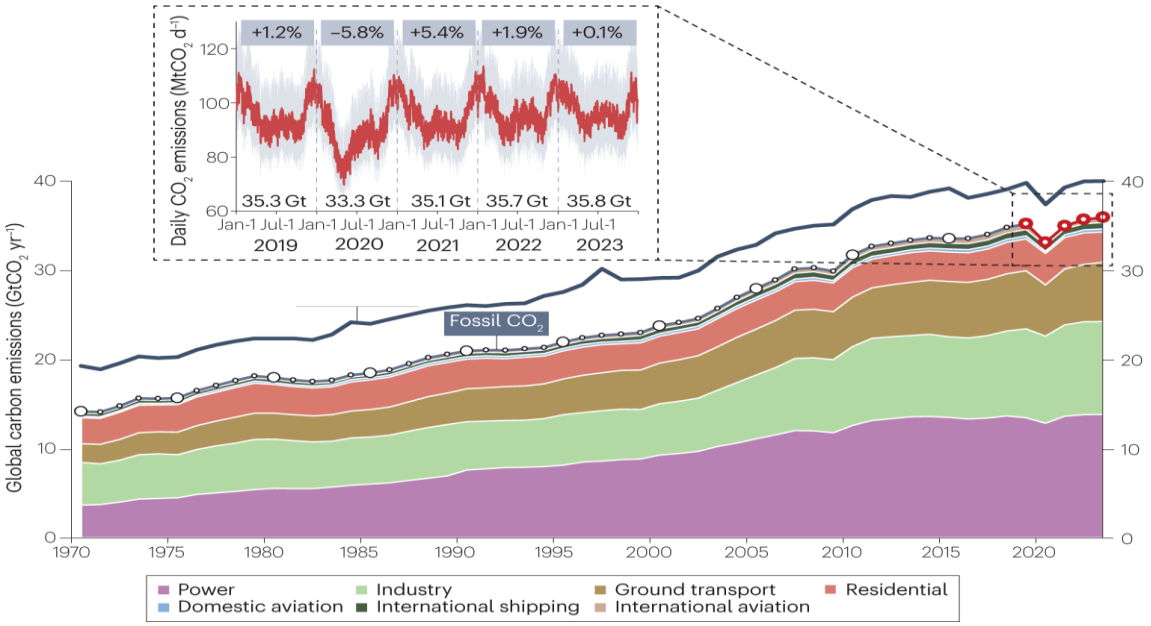

Figure 2 - Main contributors for the increase of CO_2 emissions over the years (adapted from [4])

To reduce greenhouse gas emissions, more sustainable technologies and fuels need to be developed and incorporated [5]. Namely, vegetable oils and biomass can be used to produce biodiesel with hydrochar from raw materials such as fruit peels [5]. It is an alternative form of production that has been growing over time, which makes it possible to reduce production costs, as well as utilize raw materials that would no longer serve any purpose, and transform them into value-added products [5].

Fruit trees such as banana trees are usually cultivated due to the high consumption of bananas, with an average annual intake per person of 12kg worldwide [6,7]. However, as the peels are not consumed, a large amount of waste is generated, representing around 40% of the net weight of bananas [6,7]. Banana peels (BP) contain carbon-rich compounds and a high content of inorganic elements, around 11.54% on a dry basis [7]. Banana peel chemical composition on a dry basis is as follows: it contains 9.8% ash, 12.1% cellulose, 10.2% hemicellulose, and 2.9% lignin, and it can be converted and used for various purposes, including the production of bioplastics, organic fertilizers, biofuels, and activated carbons [7,8]. Another fruit that is widely grown around the world is orange, and it is estimated that global production exceeds 55 million metric tons, generating a large amount of waste that is not used [9]. The chemical composition of orange peel on a dry basis is as follows: it contains 2.9% ash, 14.4% cellulose, 10.9% hemicellulose, and 1.3% lignin [10]. Orange peel (OP) waste represents almost 50% of the fruit's wet weight and therefore needs to be treated, otherwise, it can cause major environmental problems and economic losses for the citrus industry [9].

Lignocellulosic and non-lignocellulosic biomass can be incorporated into various thermochemical processes, such as pyrolysis, gasification, and hydrothermal carbonization [11]. Hydrothermal carbonization (HTC) is a thermochemical process that converts organic matter into simpler chemical compounds [6]. On the other hand, the natural carbonization process can take millions of years, while HTC requires just a few hours to transform biomass into a material with similar characteristics [6]. The hydrochar produced through thermal carbonization has stood out as a catalyst for transesterification and esterification reactions, and can also be used for energy storage, as well as in the medical field [11]. A reported promising example was the use of coconut endocarp combined with potassium hydroxide for the production of biodiesel, which showed superior results compared to other catalysts obtained by different thermochemical processes [11].

Figure 3 correlates keywords from scientific publications on the hydrothermal carbonization of residual biomass, through the Web of Science data website. The keywords presented include terms such as banana or orange peels and different types of biomasses, combined with different processes such as hydrothermal carbonization, gasification, or torrefaction. All these keywords data, from different scientific articles, were exported and used via VOS Viewer to produce Figure 3. Notably, the figure highlights the prevalence of agricultural waste, underscoring the emphasis on sustainable waste management practices. Additionally, it illustrates the diverse applications of these processes in converting biomass into valuable biochar, biofuels, and other bioproducts. This visualization underscores the interconnected nature of various biomass types and treatment methodologies, reflecting the multifaceted approach to bioresource utilization and environmental sustainability.

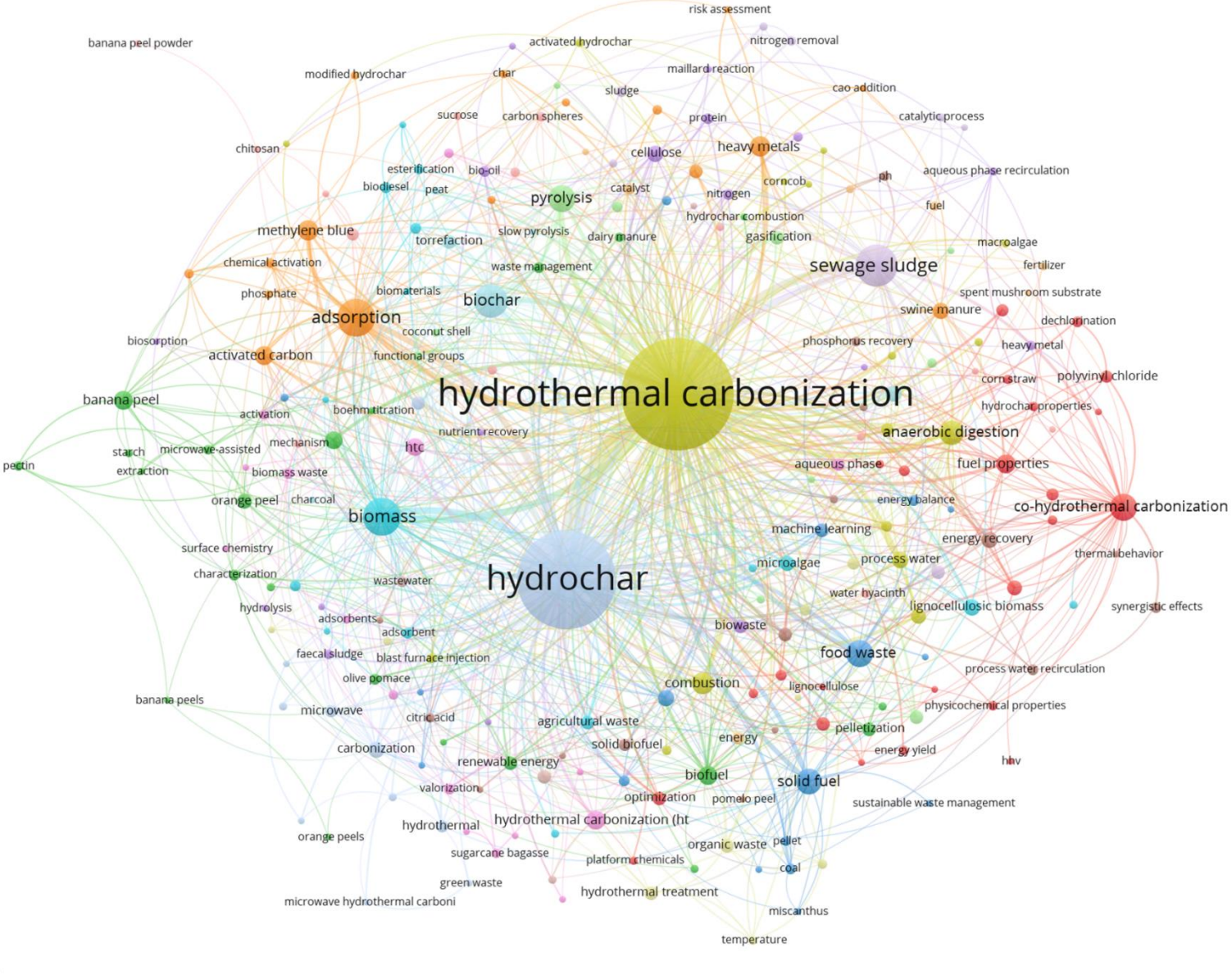

Figure 3 - Bibliometric study on hydrothermal carbonization through the use of hydrochar made from orange and banana peels in VOS Viewer software, with data exported from Web of Science (adapted from [12])

2. STATE OF THE ART

2.1. HYDROCHAR SUGAR CATALYST

2.1.1. DEFINITION, FEEDSTOCKS AND PRODUCTION

Biochar is a material consisting mainly of carbon, oxygen, and hydrogen, which can be produced through various processes such as pyrolysis, carbonization, liquefaction, or hydrothermal carbonization (if a hydrochar is to be produced) [13]. Hydrochar is defined as a carbon-rich material produced through the hydrothermal carbonization of biomass [14]. Compared to biochar produced from pyrolysis, hydrochar usually has aliphatic and less aromatic structures, and also has a greater number of functional groups on its surface, due to the different reaction conditions, such as temperature, heating rate, and reaction time [15,16]. Figure 4 shows the differences between the type of biomass used in pyrolysis and hydrothermal carbonization processes, and the product's characteristics.

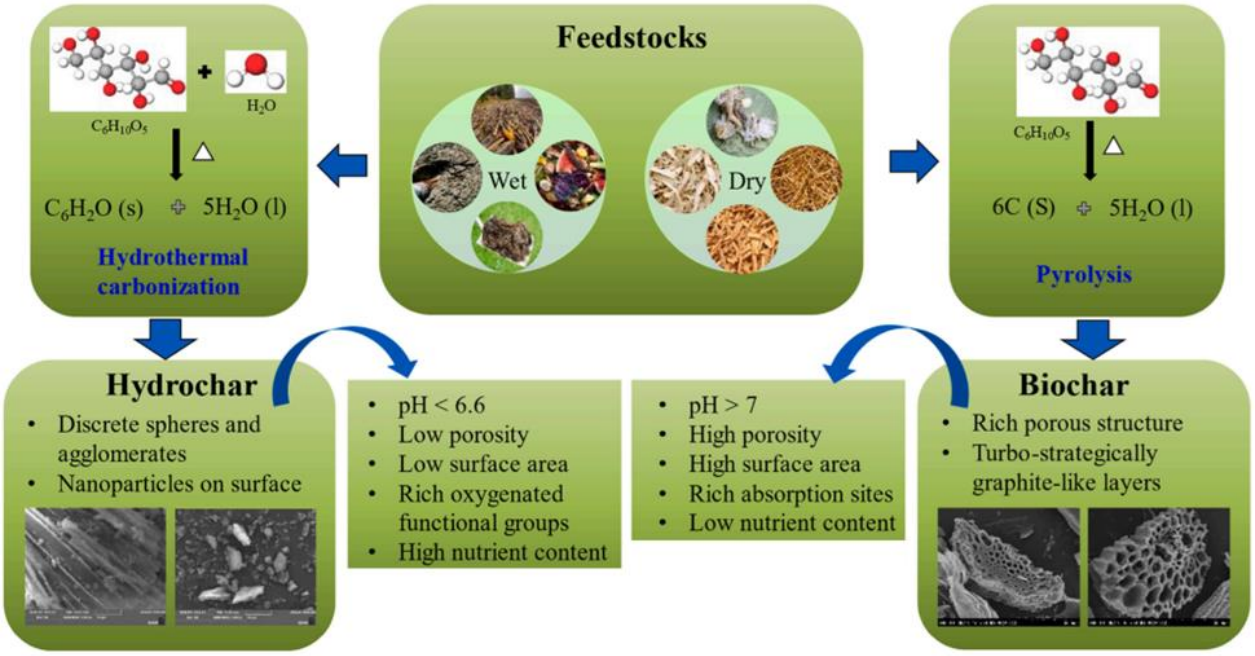

Figure 4 - Differences between the hydrothermal carbonization and pyrolysis for the manufacturing of char (adapted from [17])

Hydrochar exhibits a diverse array of agglomerates within its structure and features nanoparticles on its surface, unlike biochar, which is characterized by well-defined graphite layers and a highly porous architecture [17]. Beyond the morphological distinctions between the coals produced, hydrochar tends to be acidic, whereas biochar is generally more alkaline and boasts a higher surface area [17]. Furthermore, production processes such as hydrothermal carbonization for hydrochar and pyrolysis for biochar can also contribute to their distinct physical and chemical properties, thereby determining their suitability for various environmental and agricultural applications [17].

The properties of both biochar and hydrochar have significant potential in combating soil contamination, with hydrochar surfaces exhibiting a particularly high concentration of functional groups such as hydroxyl (-OH), carbonyl (-C=O), and carboxyl (-COOH). These functional groups are highly effective in the adsorption of inorganic and organic pollutants, enhancing the material's capacity for environmental remediation [18]. Table 1 shows some raw materials used to produce hydrochar samples, as well as the characteristics of the final product in terms of yield, carbon percentage, and the reaction conditions used to obtain the final product [15]. It can be seen that the temperature of the reaction is directly proportional to the percentage of carbon obtained since an increase in temperature leads to a higher percentage of carbon (C) [15].

Table 1 - Influence of different feedstocks on the characteristics of hydrochar (adapted from [15])

Feedstock	T (°C)	t (min)	Hydrochar Yield (wt.%)	Carbon (%)	Atomic H/C Ratio
Chinese fan palm	180	60	51	55.9	1.64
	210	60	57	58.1	1.60
	240	60	50	64.1	1.5
Bamboo shoot shell	210	30	56.4	51.3	-
	270	30	31.9	>52	-
Corn cob residue	250	35	46.6	61.7	0.08
	250	35	45.7	63.6	0.07

Table 2 illustrates the different types of carbohydrates, subdivided by their degree of polymerization, with the main subgroups being defined as monosaccharides, disaccharides, and polysaccharides.

Table 2 - Division of carbohydrates in subclasses through the degree of polymerization (adapted from [19])

Feedstock	Degree of polymerization	Subgroup	Main components
Sugars	1-2	Monosaccharides	Fructose, glucose, galactose
		Disaccharides	Sucrose, lactose, maltose
		Polyols (sugar alcohols)	Xylitol
Oligosaccharides	3-9	Maltooligosaccharides	Maltodextrins
Polysaccharides	≥10	Starch	Amylose, amylopectin
		Nonstarch polysaccharides	Cellulose, hemicellulose, pectin

Carbohydrates (CH) are defined as an important class of natural macromolecules made up of three elements, carbon, hydrogen, and oxygen [20]. These compounds are the most abundant group of organic materials found in living organisms [20]. They are produced by photosynthesis reactions between carbon dioxide and water. The common structure of CH consists of aldehydes or ketones linked to a variable number of hydroxyl groups [20].

According to their size, carbohydrates are classified into three large groups, as illustrated by the table above. Monosaccharides, made up of just one monomer, are the simplest type of carbohydrate. These are commonly known as simple sugars, such as fructose, which is found in various fruits, and contain three to seven carbon atoms, which serve as building blocks for larger molecules [20,21].

Disaccharides are made up of two monomers, such as sucrose, which is produced naturally in various plants, while polysaccharides have several units, such as starch, which is present in the structure of various plants or vegetables and allows different forms of glucose to be stored [20]. Figure 5 illustrates the different molecules of each of the types of carbohydrates mentioned above, to highlight the differences between the monomeric units of each CH.

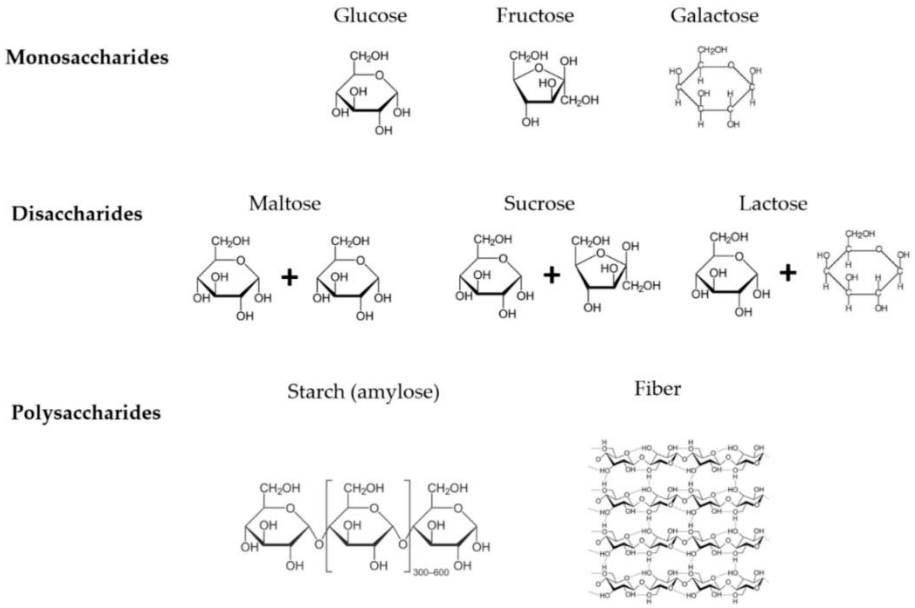

Figure 5 - Examples of different type of carbohydrates (adapted from [21])

The typical structure of lignocellulosic biomass is made up mainly of cellulose, hemicellulose, and lignin, and these three polymers are responsible for the formation of microfibers, which are essential for obtaining macrofibres to allow the cell wall to be structurally stable [22]. Cellulose is the main component of lignocellulosic biomass. It is resistant to degradation because of the bonds between hydrogen and the polysaccharides found naturally in the biomass, while hemicellulose is a natural polymer of sugars (e.g. glucose, xylose, arabinose, galactose and mannose), and lignin is made up of three phenolic materials [22].

Furthermore, chemicals can interact with biomass at elevated temperatures, facilitating the removal of a portion of hemicellulose and/or lignin. This process significantly enhances the characteristics of the remaining solid material, making it more suitable for the production of paper, particleboard, and various other products [22]. Notably, the cellulose and hemicellulose fractions of biomass, which typically constitute approximately 40 to 50% and 20 to 30% of plant matter, respectively, are complex polysaccharides [23]. These polysaccharides can be decomposed into simpler sugars through hydrolysis, utilizing either enzymatic or acidic methods [23]. These resultant sugars can then be fermented or chemically transformed into valuable fuels, chemicals, or hydrochars [23].

2.1.2. Production Methods

Hydrothermal processes are defined as thermochemical techniques that take place at high temperatures under controlled pressure. In this way, various reactions take place that alter the chemical properties of water, producing fuels and value-added chemical products [24]. Depending on the temperatures to be applied and the desired final product, hydrothermal processes can be subdivided into three processes: hydrothermal carbonization (HTC), hydrothermal liquefaction (HTL), and hydrothermal gasification (HTG), as can be seen in Figure 6 [24,25].

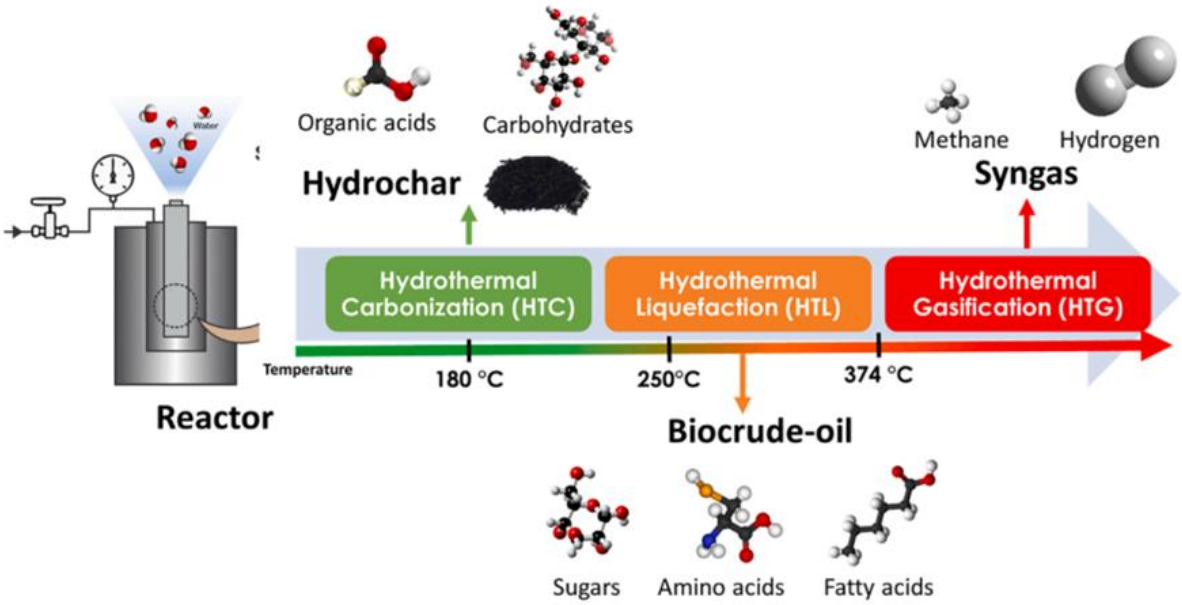

Figure 6 - Types of hydrothermal processes and its products (adapted from [24])

Hydrothermal carbonization is a thermochemical process that converts biomass with high moisture content into hydrochar at temperatures between 150°C and 230°C. This process takes place over a relatively short residence period, which can vary from minutes to hours. The conversion is carried out in the presence of water and under controlled pressure [17]. The steps that make up the production of hydrochar through HTC involve hydrolysis, dehydration, decarboxylation, polymerization, and finally carbonization [14].

The components of biomass, when subjected to the hydrolysis reaction, break down into smaller molecules in the presence of water [14]. The water molecules are then removed from the smaller molecules found in the biomass [14]. In the decarboxylation stage, the carboxyl group present in the biomass is removed, releasing CO_2, and thus forming aromatic compounds [14]. In polymerization, the carbon-rich compounds undergo polymerization reactions, forming cross-links between the polymer chains [14]. Finally, through heating and pressure, the carbonaceous compounds are carbonized, forming hydrochar [14].

HTC is a highly promising thermal technology due to its efficient conversion rate and the advantage that raw materials can be processed directly in their wet state, eliminating the need for pre-drying [17]. This makes it particularly suitable for handling residual biomass such as fruit peelings, nut shells, and other organic waste. The ability to process wet biomass not only reduces energy consumption but also streamlines the overall processing workflow [17].

Hydrothermal liquefaction is a process that converts wet biomass into bio-oil with or without the presence of a catalyst [26]. The process uses algae as biomass, from which the solid components are removed to obtain crude bio-oil [26]. The HTL process is similar to pyrolysis, but pyrolysis is a process that converts dry biomass and uses very high temperatures, between 450°C and 600°C, while HTL requires much lower temperatures, around 230°C to 370°C, to achieve appreciable yields [26,27,28]. HTL therefore has lower energy costs compared to the pyrolysis process [26,27].

Hydrothermal gasification is defined as an endothermic process in which wet biomass is treated with water at high temperatures and high pressure to produce combustion gases rich in hydrogen or methane [29]. This process reduces the amount of pollutants, such as nitrous oxides, compared to other conventional methods, since the operating temperature used is lower [29]. As mentioned above, some of the differences between pyrolysis and hydrothermal treatment technologies can be seen in Table 3.

Figure 7 illustrates the various processes by which hydrochar can be produced. Undissolved lignin can undergo pyrolysis, transforming into polyaromatic hydrochar, characterized by its complex aromatic structures. In contrast, dissolved lignin (oligomers) undergoes hydrolysis or alkylation reactions, leading to the formation of phenolic or aromatic compounds [30].

These compounds subsequently undergo polymerization reactions, resulting in the creation of aromatic oligomers, also referred to as hydrochar [30]. The versatility of these processes highlights the adaptability of HTC in converting different forms of lignin into valuable carbon-rich materials [30]. This conversion is essential for optimizing the use of lignocellulosic biomass, improving the overall efficiency of biomass utilization [30]. Furthermore, the resulting hydrochar, with a rich aromatic content, holds potential for various applications, including soil improvement, carbon sequestration, and as a precursor for advanced materials [30].

Table 3 - Differential characteristics of hydrothermal processes vs pyrolysis (adapted from [17,28])

	Hydrothermal treatments			Pyrolysis		
	HTC	HTL	HTG	Slow	Fast	Flash
Temperature	150 - 230°C	230 - 370°C	370 - 700°C	300 - 550°C	450 - 600°C	750 - 1000°C
Time	minutes - hours	1min - 120min	30s - 30min	hours - weeks	<1min	<30min
Pressure	2 - 6 MPa	10 - 25 MPa	20 - 50 MPa	0.1 MPa	<5 MPa	<0.5 MPa
Main product	Hydrochar	Bio-oil	Syngas	Biochar	Bio-oil	Pygas
Feedstock	Dry: Agricultural wastes; woody wastes. Wet: Fresh vegetable wastes; algae.			Dry: Agricultural wastes; woody wastes; algae.		

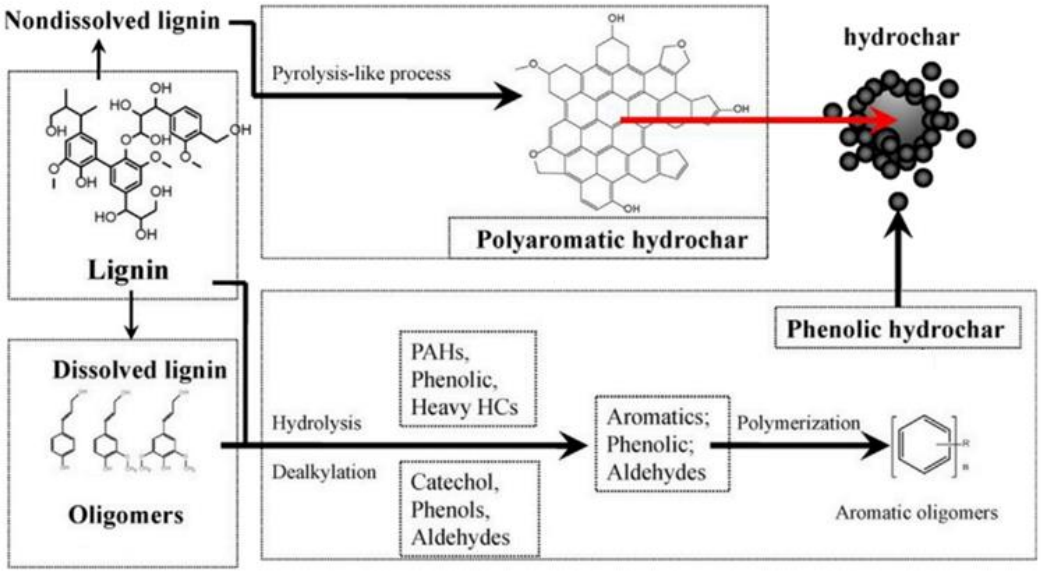

Figure 7 - Routes of production for hydrochar by lignin present in biomass (adapted from [30])

2.1.3. CHARACTERIZATION METHODS

The methods for characterizing hydrochar fall into three main categories: physicochemical, structural, and surface [31]. Each of these categories encompasses different techniques and parameters, as can be seen in Figure 8, that are fundamental for analyzing the hydrochar.

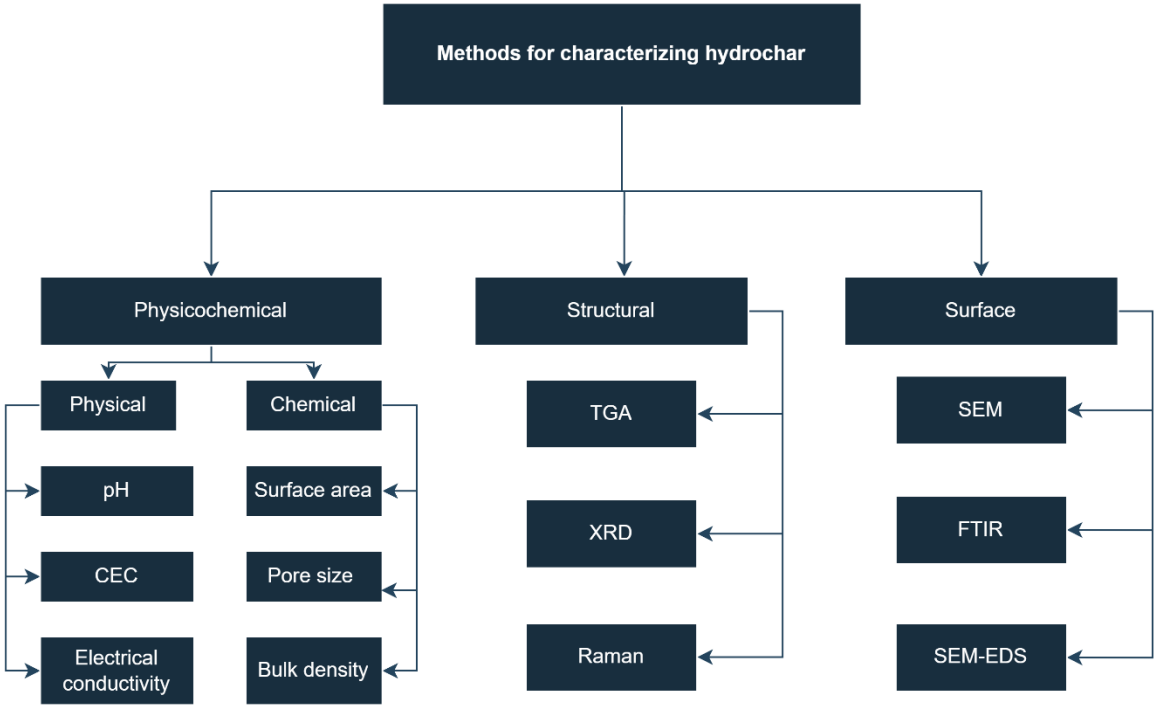

Figure 8 - Characterization techniques of hydrochar (adapted from [31])

The Scanning Electron Microscope (SEM) is one of the methods used to analyze images of micro and nanoparticles in solid objects [32]. This device makes it possible to analyze the size of particles with a resolution of up to 10 nm [32]. The SEM operates using a high-voltage system [32]. The electron beam is initially focused by passing through electromagnetic apertures and lenses and then directed onto the surface of the sample with the help of scanning coils [32]. The images are produced from the signals obtained in the area of interaction between the beam and the sample [32]. The electrons emitted by the sample are collected by an appropriately positioned detector, allowing detailed images to be formed [32].

SEM-EDS is generally suitable for analyzing elements with an atomic number greater than 11, but when a special detector for light elements is introduced, the method allows the identification of elements with an atomic number higher than 5 [33]. This method is therefore relevant for identifying explosive molecules, which often contain nitrogen atoms. SEM-EDS is particularly suitable for identifying metals [33].

Fourier transform infrared spectroscopy (FTIR) provides information on the presence or absence of specific functional groups, as well as the chemical structure of polymeric materials. The variations in the frequency of the absorbance bands and the intensity indicate changes in the chemical structure or the environment around the sample. This method can be used to determine the chemical composition of the surface, especially after chemical or physical modifications [34].

X-ray diffraction (XRD) provides crucial information that complements various microscopic and spectroscopic methods [35]. This method makes it possible to identify phases, sample purity, crystal size, and, in some cases, morphology [35]. The data obtained can be correlated with microscopy data, making it possible to check whether the microscopic observations of a small number of particles are representative of the majority of the sample [35]. X-ray diffraction is a crucial technique for studying amorphous and semi-crystalline materials [36].

Thermogravimetric analysis (TGA) can measure parameters such as moisture loss, decarboxylation, pyrolysis, solvent loss, oxidation, and decomposition of biomass or other substances [37]. In addition, thermogravimetric analysis accurately measures the thermal stability and decomposition behavior of materials, such as the rate of decomposition during the material's heating and cooling cycles [38]. This instrument can identify the minimal presence of volatile molecules, such as water and residual solvents, produced during the heating of polymer samples [38].

Raman spectroscopy is based on the scattering effect and analyses the scattering spectrum at different frequencies of light to obtain information on molecular vibration and rotation [39] It is a non-destructive analytical technique based on the interaction of light with the chemical bonds of materials [39]. Raman spectroscopy can provide detailed information on the chemical structure, phase, morphology, crystallinity, and molecular interactions of a sample [39].

2.1.4. APPLICATION

Hydrochar has several applications, ranging from the energy sector to soil remediation [40]. Figure 9 illustrates some of the applications for carbon produced through hydrothermal treatment. As depicted, hydrochar can be employed for the extraction of industrial dyes from polluted effluents; for the sequestration of carbon and other atmospheric gases; for the bioremediation of contaminated soils; for integration into agriculture as an alternative to traditional soil; for energy production or incorporation into biofuels (bio-oil) processes within biorefineries; or as activated carbon to facilitate catalytic reactions [40]. By synthesis, hydrochar can be utilized in advanced water purification systems, as an adsorbent for pharmaceutical contaminants, and in the synthesis of high-performance materials for environmental sustainability [40]. Its broad utility underscores its potential as a transformative and multifaceted resource in the domains of environmental engineering and green technology [40].

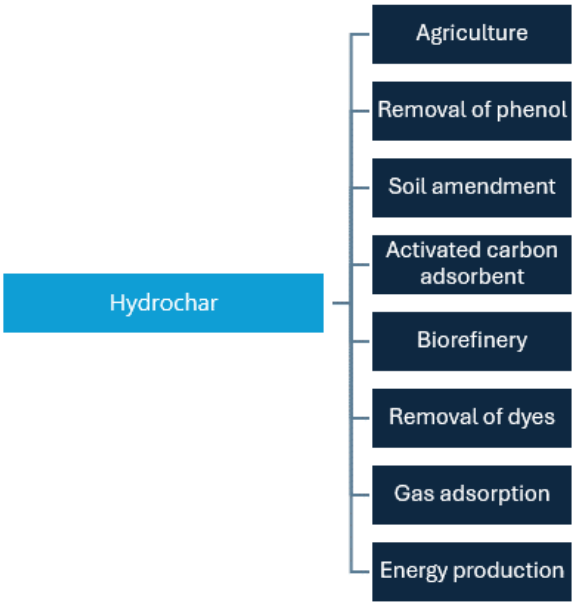

Figure 9 - Applications of hydrochar (adapted from [40])

As reported, hydrochar is effective for sorbing different polar and non-polar organic pollutants found in the soil, due to the presence of alkyl and aryl groups [41,42]. Hydrochar is also proving to be a viable alternative for the removal of heavy metals and cyclic aromatic hydrocarbons from municipal solid waste effluents, as these contaminants accumulate in their structure due to changes caused in the structure by high temperatures during hydrocarbonization processes [41]. Figure 10 shows some of the contaminants that can be adsorbed by hydrocarbons, as well as the difference this removal can make to a water sample.

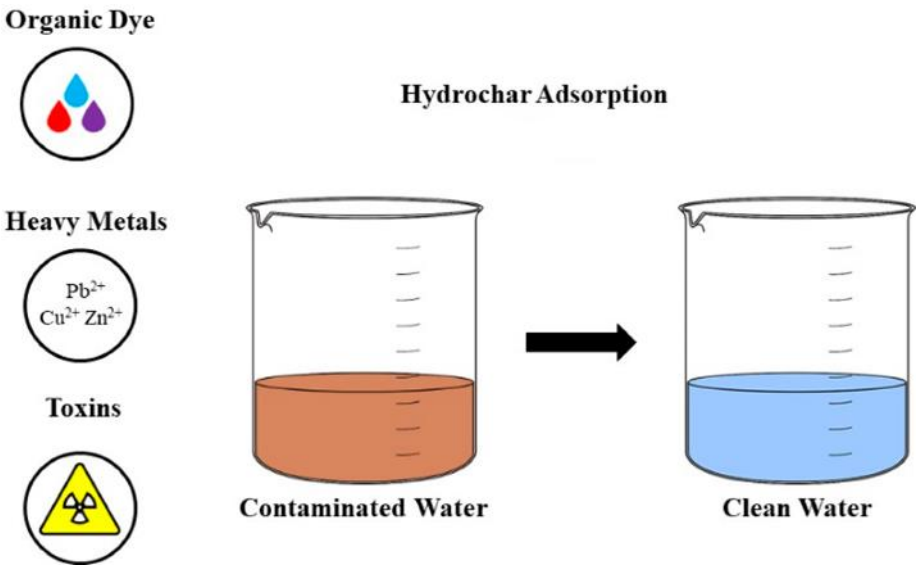

Figure 10 - Visual representation of the influence in hydrochar applications for contaminated water (adapted from [43])

In addition to removing pollutants, hydrochar can be used as a solid fuel, through the synthesis of fuel cells; electrode supercapacitors; or batteries, to convert or store energy, and hydrochar can also be burnt to obtain energy [44,45,46].

2.2. Esterification Reaction

2.2.1. Mechanism And Type Of Catalysis

Esters are found everywhere as natural and synthetic organic compounds. Esterification between alcohols and carboxylic acids is widely employed in the synthesis of organic compounds including biodiesel, which is a mixture of fatty acid esters [47]. Biodiesel are produced through either transesterification or esterification. Transesterification involves the reaction of triglycerides with an alcohol in the presence of a catalyst, while esterification utilizes fatty acids as starting materials [48]. In the transesterification, glycerin is co-produced with biodiesel [49]. Triglyceride is based on a glycerin molecule linked to three long-chain fatty acids (Figure 11).

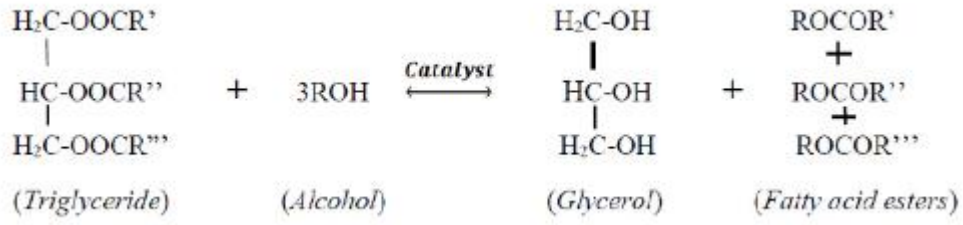

Figure 11 - Transesterification reaction for biodiesel and glycerin production (adapted from [50])

Glycerin is a by-product of this reaction, with a higher density than biodiesel, and it is necessary to separate and can ultimately be purified to be used in other industries, such as pharmaceuticals, and cosmetics, among others [50]. On the other hand, Fisher esterification transforms carboxylic acids and alcohol into esters and water (Figure 12) [47].

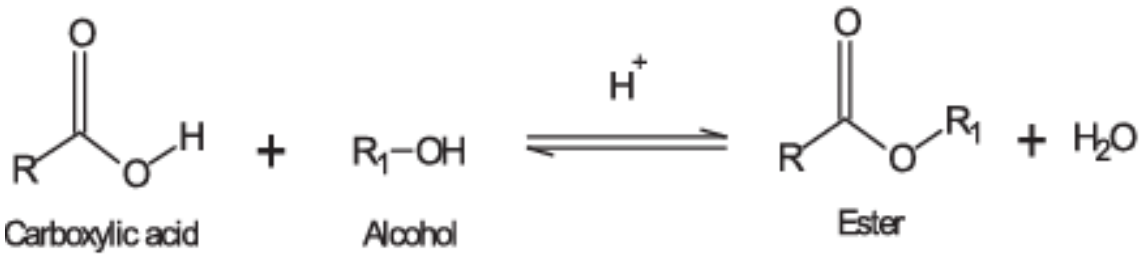

Figure 12 - Fischer-esterification reaction (adapted from [47])

After a certain period, the reaction reaches equilibrium based on kinetics and thermodynamics. To shift the equilibrium towards complete ester formation, either an excess of alcohol or continuous removal of water is typically required [47].

Heterogeneous catalysts have garnered significant interest in scientific research, particularly in the context of biodiesel production [51]. Given the increasing demand for sustainable alternatives to fossil fuels, biodiesel emerges as a promising option due to its environmental benefits [51]. The use of solid heterogeneous catalysts could provide a viable solution to reduce these costs by enhancing the efficiency of the production process, thus making biodiesel a financially competitive alternative [51].

Heterogeneous catalysis has several stages during a reaction, in which the reactants initially contact with the surface of the catalyst and external diffusion takes place, i.e. transport of the reactants from the fluid phase to the surface of the catalyst particle [51]. The reactants then move into the pores of the catalyst particle and internal diffusion takes place, but it competes with the reaction since external mass transfer depends on the thickness of the stagnant film and the activity in the outer layer [51,52]. Thus, the diffusion of molecules is hindered by physical characteristics, as well as by molecules [51,52].

The next step in the heterogeneous catalysis reaction involves the adsorption of reactants on the active center of the catalyst, followed by the formation or conversion of various adsorbed species, with reactions taking place on the surface [51]. The fifth stage involves the desorption of products from the active center of the catalyst, followed by the transport of the products through the pores to the outer surface of the catalyst particle, and finally, these products move into the fluid phase [51]. Figure 13 illustrates the steps involved in the catalytic process mechanism.

It should be noted that three of the stages are sequential: adsorption, surface reaction and desorption [52]. However, during a chemical reaction on the surface, internal diffusion is equal to the rate of the reaction in a steady state [52].

Otherwise, if the steps (1;2;6;7) that can be seen in Figure 13 are too fast, both the surface of the particle and that which goes to the active center of the pore are left without resistance for the transfer of mass from the volume [52]. It can be added that the reaction speed is not affected by the mass transfer steps when the concentration of the catalyst in the active centers is equal to that of the mass [52]. Homogeneous catalysis is characterized by a catalytic system in which the reactants and the catalyst are present in the same phase, typically liquid [53]. This process allows for the formation of a homogeneous mixture, which can lead to enhanced reaction rates and uniform catalytic activity [53]. Additionally, a more contemporary definition emphasizes the use of organo-metallic complexes as catalysts in homogeneous catalysis, where a direct bond between a carbon atom and a metal is often integral to the mechanism [53].

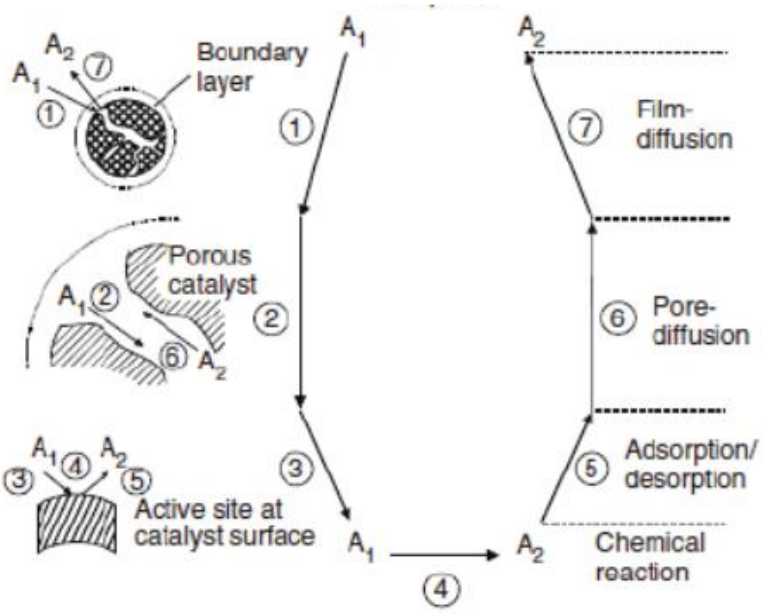

Figure 13 – Generic mechanism for a heterogeneous catalyzed reaction (adapted from [52])

This definition highlights the importance of metal-carbon interactions in facilitating catalytic transformations, although establishing such bonds may not always be feasible depending on the nature of the reaction and the catalyst employed. Homogeneous catalysis thus embodies a sophisticated approach, integrating both molecular design and phase compatibility to optimize reaction conditions and outcomes [53]. In the production of biodiesel via the esterification reaction, heterogeneous catalysis is predominantly favored due to its numerous advantages over homogeneous catalysis. One notable benefit is the ease of catalyst recovery and reuse, which significantly reduces operational costs and environmental impact [53]. Additionally, heterogeneous catalysis minimizes the likelihood of soap formation, a common byproduct in biodiesel synthesis that can complicate downstream processing [53].

Conversely, while homogeneous catalysis can achieve higher conversion rates and greater reaction efficiency, it is often associated with challenges such as the generation of toxic byproducts and an increased risk of equipment corrosion [54]. These disadvantages arise from the potential for catalyst leaching and the corrosive nature of acidic or basic reaction conditions used in homogeneous systems, which can compromise the integrity of processing equipment and necessitate more stringent safety measures [54].

2.2.2 REACTIONAL PARAMETERS

2.2.2.1 FEEDSTOCKS

Biodiesel is made up of fatty acid esters, and to obtain it, it is necessary to analyze the ester profiles of biodiesel [55]. The main raw materials for biodiesel production come from vegetable oils [55]. Vegetable oils are made up of triglyceride molecules composed of a glycerin molecule linked to three fatty acid chains [55]. The fatty acids found in vegetable oils usually have between fourteen and twenty-two carbon atoms, although there can be some variations in their length [56]. The most common fatty acids are oleic, linoleic, palmitic, and stearic, with oleic acid being the most widely used [57,55]. Palmitic and stearic acids are saturated fatty acids and therefore do not have double bonds in their molecular structure [55]. Oleic acid is monounsaturated, and linoleic acid, since it has two double bonds in its structure, is polyunsaturated [57].

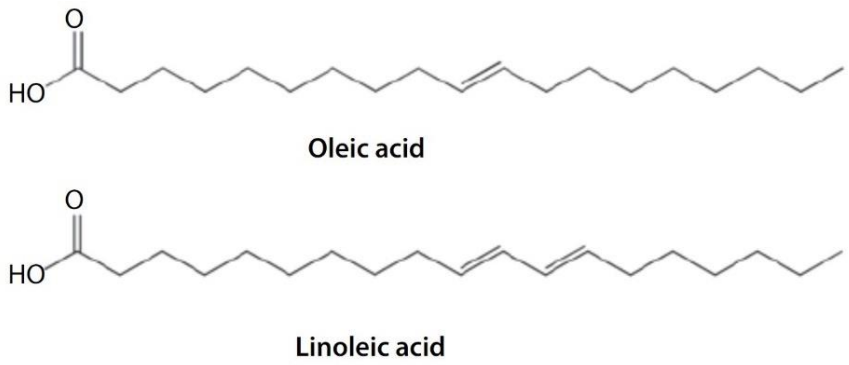

Figure 14 - Examples of known fatty acids (adapted from [56])

For the production of biodiesel, the best vegetable oils to use are the ones with a monounsaturated group, since polyunsaturated fatty acids have poor oxidation stability and can alter the kinematic viscosity, compromising the properties of the fuel as well as its quality, also the density and cetane number of the biodiesel can be affected [55]. Table 4 shows the detailed fatty acid composition of different raw materials, including rapeseed oil, used frying oil, yellow fat (defined as a fatty product that does not meet the definitions of animal fat, vegetable fat or oil, hydrolyzed fat, or a fat ester), brown fat (contains a wide variety of solid food residues and suspended wastewater), sunflower oil, palm oil and jatropha oil [58,59].

Fatty acids are identified by the number of carbon molecules, as well as the level of saturation. Palmitic acid has sixteen carbons, and the number zero after, since it is saturated [60]. Oleic acid (OA), on the other hand, has eighteen carbons, and the fact that it is monounsaturated means that it has the number one, while linoleic acid has eighteen carbons and is polyunsaturated [60].

Table 4 - Fatty acids composition of different vegetable oils of feedstocks (adapted from [60])

Feedstock	Fatty acids (wt.%)			
	Palmitic (16:0)	**Stearic (18:0)**	**Oleic (18:1)**	**Linoleic (18:2)**
Rapeseed	3.49 – 4.0	0.55 – 2.3	62 – 77.8	14.1 – 32
Soybean	—	2.6 – 4.7	16.5 – 24.8	52.3
Waste frying oil	12	53	33	3
Yellow grease	3.79	12.96	44 – 32	6.97
Brown grease	3.13	12.54	44.36	12.09
Sunflower	—	22.52	22.52	52.34
Olive palm kernel	18.8	10.2	17	2.2
Jatropha	—	—	38.6 – 44.7	32.8 – 36

2.2.2.2 Reactant Alcohol

A solvent is any substance that has the ability to dissolve another substance, usually liquid, water is considered the “universal solvent”, but many substances are insoluble in water and therefore require liquids other than water to dissolve them [61]. There are various solvents that can be used in a wide variety of areas, such as the automotive, metallurgical and petrochemical industries and can also be obtained from the distillation of crude oil and, in these cases, present the risk of being flammable [61].

As mentioned above, solvents can have many applications, such as contributing to catalysis reactions. These reactions include the esterification reaction of fatty acids, in which a short-chain alcohol (SCA) is used [62]. Ethanol, SCA, requires a more complex production technology and a slow reaction speed [63]. In this way, methanol, another SCA, stands out in terms of low cost, because it has a shorter chain of carbon atoms and because it does not form azeotropes in the presence of water, so it is easily recycled [64]. As reported by Silva et al (2015), a reaction with methanol use, proportionate a higher chemical equilibrium constant, followed by ethanol, and only then propanol, which means that methanol is the most favorable alcohol for the oleic acid esterification [62].

Figure 15 illustrates the classical esterification reaction of a fatty acid, specifically oleic acid, in conjunction with various short-chain solvents, whereas in this reaction, the choice of solvent plays a pivotal role in determining the products, when methanol is utilized as the solvent, the resulting products are methyl oleate and water [62]. This reaction exemplifies the feasibility of, through an esterification process, synthesizing desirable esters, while generating water as a byproduct, which is typically removed to drive the reaction to completion [62].

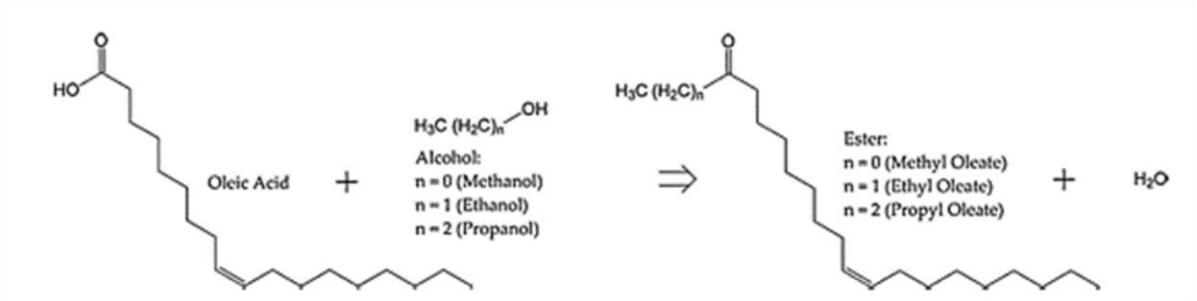

Figure 15 - Visual representation of a typical esterification reaction (adapted from [62])

If ethanol is chosen, ethyl oleate and water will be formed [62]. If propanol is chosen as the solvent, propyl oleate and water are formed [62]. It is therefore clear that the choice of solvent is intrinsically related to the product formed, due to the correlation between the number of carbons in the solvent chains and the type of oleate produced [62].

Table 5 - Properties of different solvents used in esterification reaction (adapted from [65])

Properties	Methanol	Ethanol	Propanol
Chemical formula	CH_3OH	C_2H_5OH	C_3H_7OH
Molecular weight (g/mol)	32.04	46.07	60.10
Density (kg/m^3)	791.3	789.4	803.7
Boiling point (°C)	65	79	97
Lower heating value (MJ/kg)	20.01	26.08	29.82
Vaporization latent heat (kJ/kg)	1162.64	918.42	727.88
Self-ignition (°C)	385	363	350
Latent heating (KJ/kg) 25°C	1162	904	728
Viscosity (mm^2/s) 40°C	0.59	1.13	1.74

Of the three solvents mentioned, methanol appears to be a viable choice for inclusion in a chemical reaction for several reasons, one of which is related to the boiling point [66]. Methanol, with a boiling point of 65°C, has a low bp value that allows reactions to take place at a lower temperature because methanol begins to evaporate at 65°C [66].

During solvent evaporation, the reflux process normally incorporated in many chemical reactions, such as esterification and transesterification, enables the cooled vapors to condense back into liquid form via a condenser [66]. If the boiling point of a solvent is too high, the reaction will proceed slowly, leading to higher energy consumption and longer reaction times [66].

2.2.2.3. CATALYSTS

A catalyst is a substance that accelerates the speed of a chemical reaction without interfering with the process [67]. It can modify the speed of reactions that occur thermodynamically, guiding the rate of development of the tests [67]. The presence of a catalyst has no impact on the equilibrium constant of the reaction, as it only affects the speed of the reactions [67].

The catalyst provokes a kinetic effect that provides an alternative chemical mechanism in which the reactants, under moderate conditions, are converted into products [68]. In this way, the reaction can be carried out at lower temperatures, with lower energy consumption, reducing the costs associated with energy expenditure and construction materials, as well as reducing the formation of unwanted by-products [68]. Figure 16 provides a comparison of a reaction, catalyzed and uncatalyzed, in which it can be seen that by reducing the activation energy required for the reaction to take place, the catalyst accelerates the reaction [68].

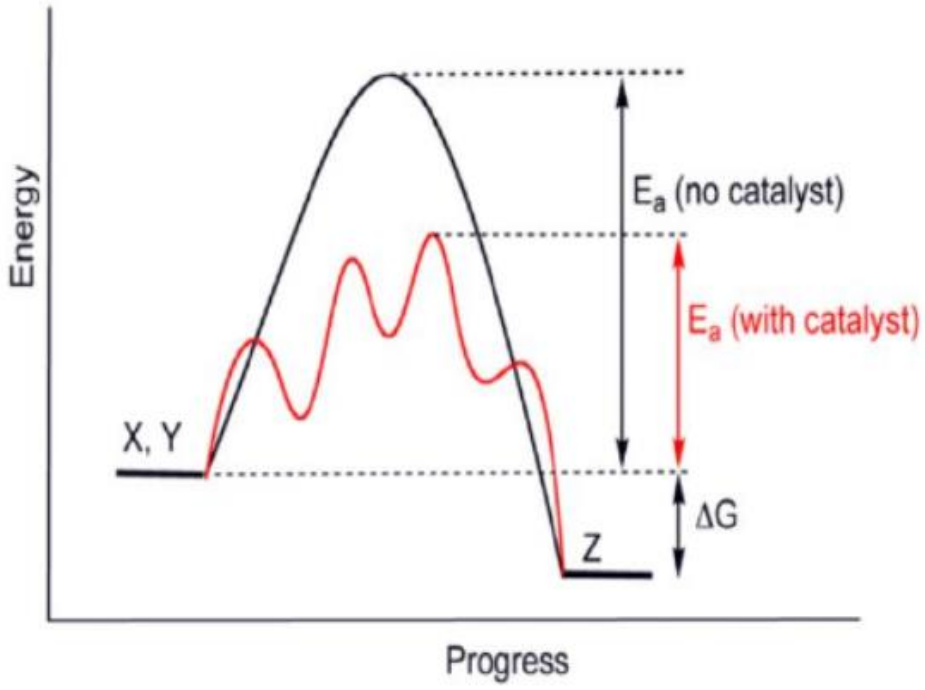

Figure 16 - Demonstration of the influence that a catalyst has in a chemical reaction (adapted from [68])

When a greater amount of catalyst is added, emulsions can form, causing the biodiesel yield to lower as its viscosity increases [67]. In the case of fatty acids, they undergo an esterification process producing water as a by-product by shifting the equilibrium in the opposite direction of the reaction [67].

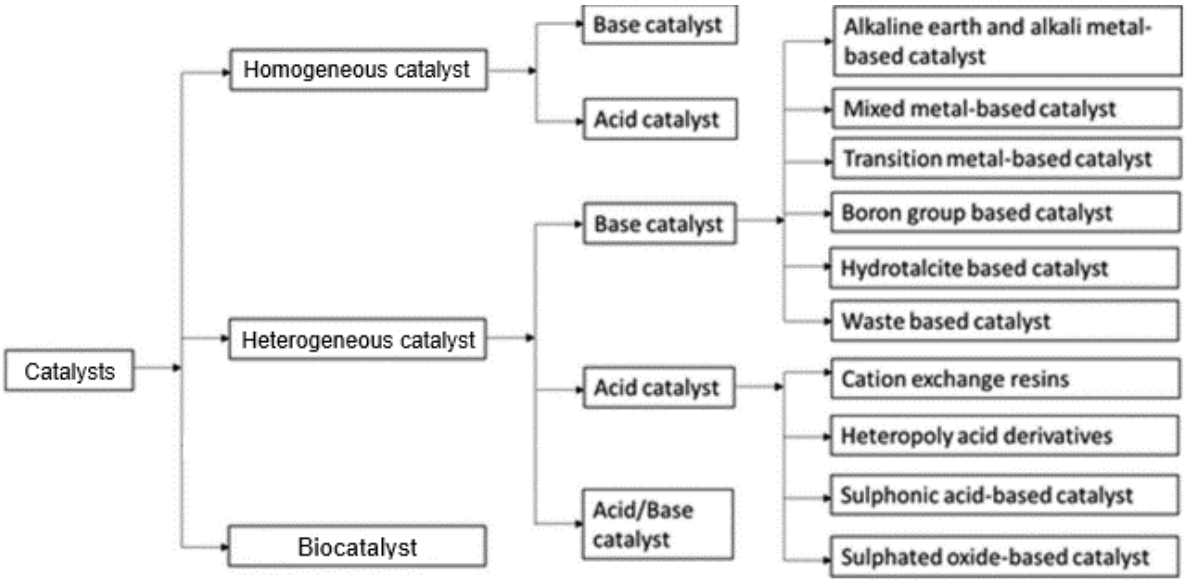

Figure 17 - Catalysts categorization according to their nature, with examples for each type (adapted from [69])

Catalysts can be divided into three main categories, homogeneous catalysts, heterogeneous catalysts, and biocatalysts, and can also be divided into subgroups such as alkaline, acidic, and enzymes, as can be seen in by changing the equilibrium in the opposite direction of the reaction [70].

Enzymatic catalysts, like biocatalysts, are constantly being developed, as they can avoid the formation of soaps and facilitate the purification progress, but they are not used commercially due to the need for longer reaction times and their high cost [70].

As for heterogeneous catalysts, they are in solid form, so that the reactants and catalysts are in two distinct phases in a reaction mixture, making it easier to separate the product, which can then be recovered and reintroduced into process [71]. In this way, they are much more economical for the synthesis of biodiesel, as well as being able to withstand high levels of moisture and fatty acids [71]. Heterogeneous catalysts can be alkaline, acid, or acid-base catalysts. However, for biodiesel production, the most commonly used are alkaline catalysts and acid catalysts [70].

Many heterogeneous alkaline oil catalysts have been developed, such as basic zeolites, alkaline earth metal oxides, and hydrotalcite. Solid-based catalysts are easily regenerated and have a lower corrosion temperature, which leads to safer, cheaper, and more environmentally friendly operations [72].

The use of heterogeneous catalysts is expected to eliminate the problems associated with homogeneous catalysts [72]. Table 6 shows some examples of different heterogeneous alkaline catalysts for various oils for biodiesel production. Furthermore, it can be concluded that through different catalysts and different reaction conditions, both the yield and the production efficiency can be affected. The right choice of catalyst and optimum conditions are crucial to maximizing the yield and efficiency of the process [72,70].

Table 6 - Examples of alkaline heterogeneous catalysts and the results of their incorporation in biodiesel reactions (adapted from [73])

Catalyst	Wt.% Catalyst	Alcohol used	Oil	Alcohol/Oil Molar Ratio	T (°C)	t (h)	Yield (%)
$Sr_3Al_2O_6$	3	MeOH	Soybean	25:1	60	1	96
$CaZn(OH)_4$	3	ETOH	Sunflower	20:1	78	3	95
K_3PO_4	5	MeOH	Fried	6:1	65	3	78
Li/CaO	5	MeOH	Karanja	6:1	65	1	99
MgO carbon based	6	MeOH	Castor	12:1	75	1	96.5

Acidic heterogeneous catalysts are insensitive to the FFA content, the biodiesel washing phase does not need to be carried out, separation of the catalyst from the reaction medium is easy, product contamination is low, regeneration is easy, catalyst recycling is easy, and even with the presence of acidic species the problem of corrosion is reduced [72].

Acid catalysts are preferred for the esterification of FFAs, when compared to alkaline catalysts, due to their higher efficiency, however, acid-catalyzed reactions require high temperatures, pressures, and a high amount of alcohol [73].

Although they provide a longer catalysis time compared to catalysis reactions with alkaline catalysts, the main advantage of acid catalysis is the efficient esterification of free fatty acids into vegetable oils with very high acidity values, such as waste cooking oil [73]. Table 7 below shows some examples of heterogeneous acid catalysts for different oils and reaction conditions.

Table 7 - Acid heterogeneous catalysts used for biodiesel production (adapted from [73])

Catalyst	Wt.% Catalyst	Alcohol	Source	Alcohol/Oil Molar Ratio	T (°C)	t (h)	Yield (%)
HZSM-5 Zeolite	10	MeOH	Oleic acid	20:1	100	7	81
30% $WO_3/AlPO_4$	5	MeOH	Soybean oil	30:1	180	5	73
Sulfonated carbon nano-horn	3	MeOH	Palmitic acid	33:1	65	5	93
Sulfated LaO	10	MeOH	Oleic acid	5:1	100	6	95.5
Sulfated LaO/HZSM-5	10	MeOH	Oleic acid	5:1	100	7	998

Homogeneous catalysts and reactants are in the same phase, i.e. they all appear as molecules in the gas phase or, more often, in the liquid phase [74]. Like organo-metallic species or enzymes, they are molecules with specific structures [75]. The active center of a homogeneous catalyst is the same for each of its molecules [75]. When the catalyst is already dissolved, the number of active centers is relatively small under normal conditions within a reactor volume, so the activity per unit volume of the reaction medium is limited [75].

Homogeneous alkaline catalysts such as sodium hydroxide (NaOH) or potassium hydroxide (KOH) are the most widely used catalysts for biodiesel production [73]. As their main advantage, these catalysts have a higher yield, obtained under moderate reaction conditions, and short reaction times [73,76]. These catalysts are suitable for oils with a low free fatty acid content, since for oils with a high free fatty acid value, they can lead to the formation of soaps [73]. In general, alkaline catalysts are widely used and effective for biodiesel production, especially with fats with a low FFA content [73]. Table 8 shows some examples of homogeneous alkaline catalysts and the optimum conditions for their incorporation into catalytic reactions.

Table 8 - Basic homogeneous catalysts used for biodiesel production (adapted from [73])

Catalyst	Alcohol	Oil	Alcohol/Oil Molar Ratio	T (°C)	t (h)	Yield (%)
NaOH	MeOH	Sunflower	6:1	60	1	97
KOH	ETOH	Soybean	12:1	60	1	95
$NaOCH_3$	MeOH	Waste frying	6:1	60	1	93
Dimethylamine (DEA)	MeOH	Cottonseed	9:1	190	3	67
KOH	MeOH	Castor	5.4:1	64	2.5	97.82

Homogeneous acid catalysts such as H_2SO_4, H_3PO_4, HCl and sulphonated acids are the most commonly used for the transesterification of vegetable oils [77]. Some of these catalysts can be seen in Table 9, along with the optimum conditions and yield for each one.

Table 9 - Acid homogeneous catalysts used for biodiesel production (adapted from [73])

Catalyst	Alcohol	Source	Alcohol/Oil Molar Ratio	T(°C)	t (h)	Yield (%)
CH_3SO_3H	ETOH	Palm fatty acid	3:1	130	1	80
$C_2HF_3O_2$	MeOH	Soybean oil	20:1	80	6	98
$NaOCH_3$	MeOH	Waste frying oil	6:1	60	1	93
H_3PO_4	MeOH	Palm fatty acid	3:1	130	1	51
H_2SO_4	MeOH	Ruce bran oil	-	100	8	97

A homogeneous acid catalyst is neutral to free fatty acids (FFA) and therefore gives better results for the transesterification or esterification of vegetable oils or fats with a high amount of FFA. At least 2% by weight acid catalysts are normally used to reduce the FFA content of used cooking oils and animal fats by esterifying them before transesterification with the aid of a catalyst [77]. However, acid-catalyzed biodiesel production has some limitations, such as a slow reaction rate and requiring a high molar ratio of alcohol to oil [77].

2.2.2.4. BIODIESEL

Biodiesel is made up of a mixture of fatty acid alkyl esters and can partially replace fossil diesel in the transport sector, thus helping to reduce anthropogenic carbon emissions [78]. It is a sustainable, biodegradable, and non-toxic substitute that can be easily produced through esterification and transesterification reactions catalyzed by bases or acids [79].

Biodiesel can be used pure or blended with fossil diesel due to its complete miscibility. Biodiesel blends are referred to as Bxx, where the xx indicates the amount of blend [80]. Thus, B100 corresponds to pure biodiesel, and a B80 blend corresponds to 80% biodiesel and 20% diesel by volume [80]. A practical example of the influence of blends is the amount of carbon monoxide emissions, with the rpm meaning the rotation per minute of the vehicle engine.

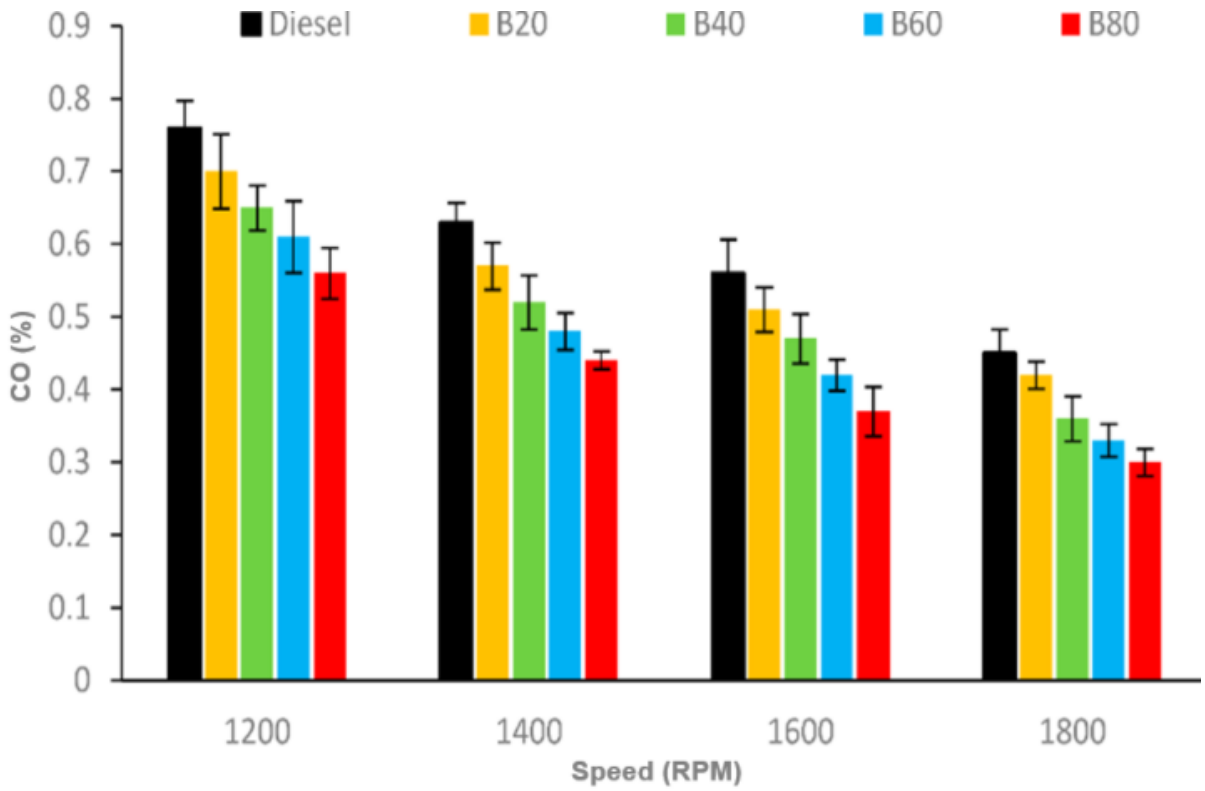

Figure 18 - Influence on carbon monoxide emissions by the increment of biodiesel in diesel blends (adapted from [81])

Figure 18 shows that the carbon monoxide emissions of biodiesel blends are lower than those of diesel at different speeds. As the proportion of biodiesel increases, CO emissions show a downward trend [81]. Currently, the maximum biodiesel incorporation rate defined by the Fuel Quality Directive for the whole of Europe is 7%, which indicates that the maximum FAME content is 7% (B7) [82].

Figure 19 illustrates some of the numerous examples of applications that biodiesel can have, from its incorporation into fuel for airplanes; buses; trains; agricultural machinery, and trucks, to its use in domestic heating [83].

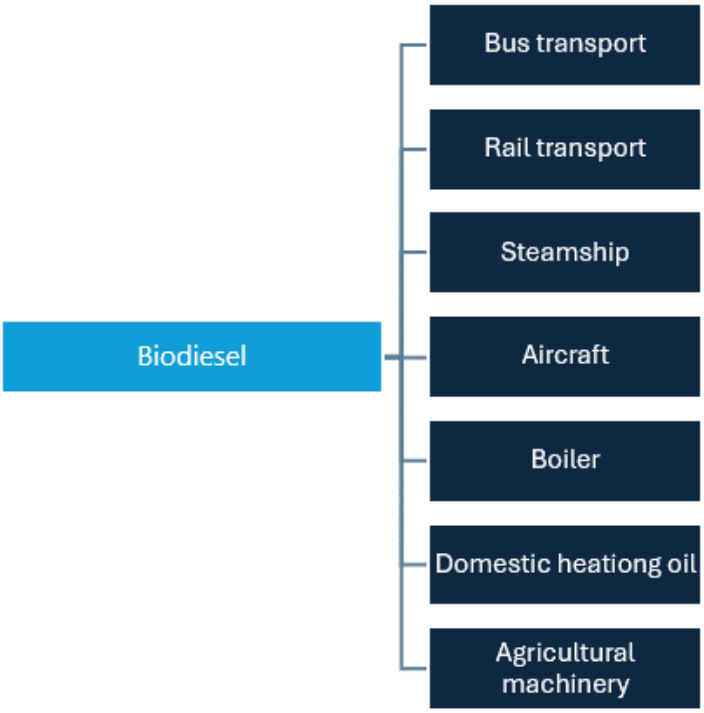

Figure 19 - Applications of biodiesel (adapted from [83])

The incorporation of biodiesel into diesel engines provides a considerable reduction in carbon monoxide (CO), unburned hydrocarbons, and particulate emissions. It also provides mixtures with a higher cetane number, which is directly related to better fuel ignition quality [84, 85]. Due to its lower emissions, biodiesel is an excellent alternative for use as a fuel for maritime (e.g. ships) and rail transportation [84].

In addition to reducing emissions, the incorporation of biodiesel has several advantages, such as the fact that it has a relatively low cost, due to the incorporation of residual material in its production (e.g. waste oils, cellulosic wood raw materials); it has better thermal efficiency, related to a reduction in friction, due to its better lubrication properties; and the fact that it makes it possible to extend the efficiency of the engine's useful life, while at the same time reducing the costs of eventual replacement [86,87, 88,89].

The chemical and physical properties of biodiesel can be influenced by various factors and can directly affect the quality of biodiesel [80]. To be marketed, it needs to comply with the quality specifications established by the Organization for Standardization (ISO) and the American Society for Testing and Materials (ASTM) [80]. Table 10 shows the requirements selected for B100, according to the standards ASTM D6751 e EN 14214 [80].

Table 10 - Required specifications for Biodiesel to be commercialized (adapted from [80])

Property Specification	ASTM D6751 Limit	EN 14214 Limit
Ester content (% (m/m))	-	96.5
Density at (15 °C (kg/m³))	880	860-900
Viscosity at (40 °C (mm²/s))	1.9-6.0	3.5-5.0
Cetane number	Min. 47	Min. 51.0
Iodine number (g I_2/10 g)	-	Max. 120
Acid value (mg KOH/g)	Max. 0.50	Max. 0.50
Pour point (°C)	-15 a -16	-
Flash point (°C)	Min. 130	Min. 101
Cloud point (°C)	-3 a 12	-
Cold filter plugging point (°C)	Max. +5	-
Copper strip corrosion (3 h at 50 °C)	No 3	Class 1
Carbon residue (% (m/m))	Max. 0.05	-
Methanol content (% (m/m))	Max. 0.20	Max. 0.20
Water content (mg/kg)	Max. 500	Max. 500
Sulfur (mg/kg)	S15 Max 15 S500 Max 500	Max. 10.0
Sulfated ash (% (m/m))	Max. 0.02	Max. 0.02
Phosphorus content (mg/kg)	Max. 10	Max. 4.0
Free glycerol (% (m/m))	Max. 0.02	Max. 0.02
Total glycerol (% (m/m))	Max. 0.24	Max. 0.25
Monoglyceride (% (m/m))	Max. 0.40	Max. 0.70
Diglyceride (% (m/m))	-	Max. 0.20
Triglyceride (% (m/m))	-	Max. 0.20
Distillation temperature, 90% recovered (°C)	Max. 360	-
Oxidation stability (h a 110 °C)	Min. 3	Min. 8
Linolenic acid methyl ester (% (m/m))	-	Max. 12.0
Polyunsaturated (≥4 double bonds) Methyl esters (% (m/m))	-	Max.1.00
Alkaline metals (Na^+ K) (mg/kg)	Max. 5	Max. 5
Alkaline earth metals (Ca + Mg) (mg/kg)	Max. 5	Max. 5
Total contamination (mg/kg)	-	Max. 24

2.2.2.5. WATER EFFECT

One of the parameters to be taken into account in the esterification reaction is the effect of water, which has been associated with decreases in the kinetics of the reaction, through a reverse hydrolysis reaction (change in the direction of the reaction, towards the direction that favors the formation of reactants) that can be caused by water, since it is co-produced with the ester, and its presence can thus lead to a decrease in the conversion of the acid [90,91]. In addition, the hydrophobicity of carboxylic acids must be considered, which tends to increase with the length of the carbon chain of these acids [90]. Not only in carboxylic acids, but also in catalysts, hydrophobicity needs to be analyzed, as this is an essential characteristic for a catalyst to be considered good for the esterification reaction, and it has been reported that catalysts with a high carbon composition have excellent hydrophobicity, however, this property can be affected by the hygroscopic nature of the sulfonic groups [92,93]. Water not only interferes with the equilibrium of the reaction but can also cause its adsorption, together with methanol, on the active centers of the catalyst, thus reducing the number of methanol-activated species for the esterification reaction [92]. It has been reported that a high-water content in carboxylic acids also causes the yield of methyl oleate to remain unchanged over a long period [92]. Figure 20 shows the effect that the presence of water can have on the yield of methyl oleate in an esterification reaction.

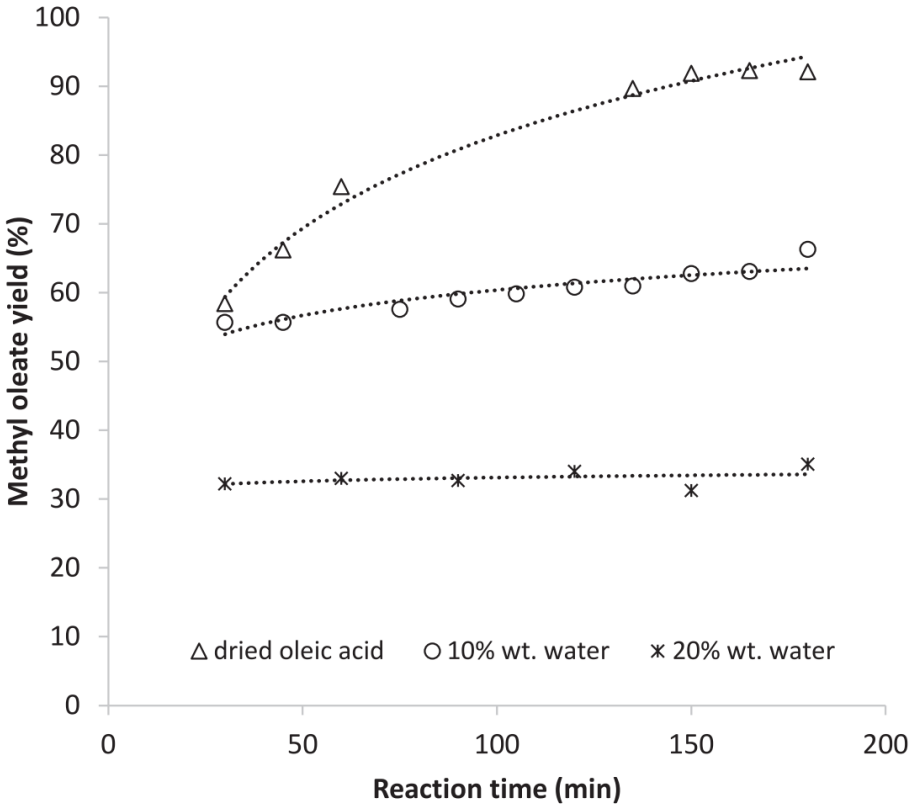

Figure 20 - Influence of the water presence on esterification reactions by the demonstration of the yield values obtained (adapted from [92])

3. METHODOLOGY

3.1. HYDROCHAR PRODUCTION AND CHARACTERIZATION

The feedstocks used for hydrochar production were cornstarch, fructose, sucrose, orange peels and banana peels. The preparation of raw materials was an essential stage in the production of hydrochar. The biomasses were divided into distinct feedstock types, and it was identified that only a selected few possessed a high moisture content, necessitating pre-treatment through oven drying. Consequently, this preparatory step was exclusively conducted on the banana peel samples, which contained 85.0% moisture, and the orange peel samples, which contained 73.5% moisture [94,95].

The process of oven drying these high-moisture biomass samples is essential to reduce their moisture content to optimal levels [96]. This not only facilitates efficient hydrochar production but also enhances the energy efficiency of the process [96]. By reducing the moisture content, the biomass become more amenable to subsequent thermal treatments, leading to a higher yield and quality of hydrochar, this step ensures uniformity in the feedstock, which is critical for achieving consistent results in hydrochar production [96]. The previous dehydration step was fundamental, to not compromise the biomass integrity, since the water content present in the biomass favors the formation of microorganisms that can deteriorate the lignocellulosic materials, such as banana or orange peels [97]. Another factor relating to the water content with biomass is due to the particle size of the sample, since the presence of water in the biomass composition can lead to a slightly higher critical arching distance between particles [98].

Through meticulous preparation and categorization of the raw materials, the overall efficiency and effectiveness of the hydrochar production process are significantly improved [94,95]. This approach underscores the importance of tailored pre-treatment methods based on the specific characteristics of each biomass type, ultimately contributing to more sustainable and economically viable hydrochar production practices [94,95].

Following the dehydration process, the dried peels were subjected to mechanical fragmentation, where they were reduced to smaller fragments and subsequently ground using a chopper to achieve a more uniform particle size distribution. For feedstocks with inherently low water content, such as sucrose, fructose, and corn starch, pre-treatment was deemed unnecessary. These materials were simply weighed and directly incorporated into the hydrothermal carbonization reaction system. Table 11 delineates each biomass sample's specific weights, and the quantities of sulfuric acid used, detailing the respective molar and mass ratios and the precise reaction conditions employed.

Table 11 – Hydrochar production conditions for different feedstocks

Feedstock	Molar mass (g/mol)	Molar sulf. ratio	Mass sulf. ratio	Weight of biomass (g)	Mass H_2SO_4 (g)	T (°C)	t (h)	Speed (RPM)
Cornstarch	692.7	1:1 1:3 1:5	-	176.6 58.8 35.3	25	150	5	730
Fructose	180.16	1:1 1:3 1:5	-	45.9 15.3 9.2	25	150	5	730
Sucrose	342.3	1:1 1:3 1:5	-	87.3 29.1 17.5	25	150	5	730
Orange peels	-	-	3:1 2:1 1:1	75 50 25	25	150	5	730
Banana peels	-	-	3:1 2:1 1:1	75 50 25	25	150	5	730

As cited before, banana and orange peels encompass a vast array of chemical compounds within their matrix, which makes it very difficult to determine the molar masses. Due to the heterogeneous and intricate nature of these organic materials, the correlation was instead established based on the mass ratio between peels and sulfuric acid. In contrast, sucrose, fructose, and starch are well-characterized carbohydrates, with sucrose being a disaccharide, fructose a monosaccharide, and starch a polysaccharide. Which makes them possess clearly defined and well-documented chemical structures. Their specific molar masses are well established, allowing for an accurate correlation with the molar mass of sulfuric acid. This precise relationship facilitates the determination of specific weights and ratios, thereby enabling a more controlled and predictable analysis of the reaction parameters.

A glass goblet equipped with a magnetic stir bar was positioned on a stirring hotplate within the fume hood, where the feedstock and H_2SO_4 were meticulously introduced. To mitigate the emission of vapors, a watch glass was placed atop the goblet. The reaction proceeded at a controlled temperature of 150°C, with continuous stirring at a rate of 730 revolutions per minute (RPM), with the pressure not having a considerable impact on the process of hydrocarbonization, since it is self-generated and primarily influenced by the initial biomass and carbonization temperature [99]. As the reaction advanced, manual agitation with a glass rod was employed to ensure uniform mixing of the heterogeneous mixture, since the resistance to stirring increased due to a growth of the thickness mixture, because of the formation of volatile products in the liquid mixture [100]. After 5 hours, hydrochar formation was completed.

However, the resultant hydrochar exhibited significant acidity, necessitating its neutralization through multiple washes with deionized water to reduce the acidity of the char that is caused by the acid added into the process [101]. Three sequential washes were performed, each followed by filtration using a vacuum pump to remove excess acidity and impurities. This purification process is depicted in Figure 21 on the left, the hydrothermal carbonization process is illustrated (labeled as 1), while the right side shows the filtration setup utilizing a Büchner funnel and vacuum pump (labeled as 2). After the completion of these washing and filtration steps, the hydrochar was carefully stored for subsequent application as a catalyst in the esterification reaction, ensuring its readiness for further use in catalytic processes.

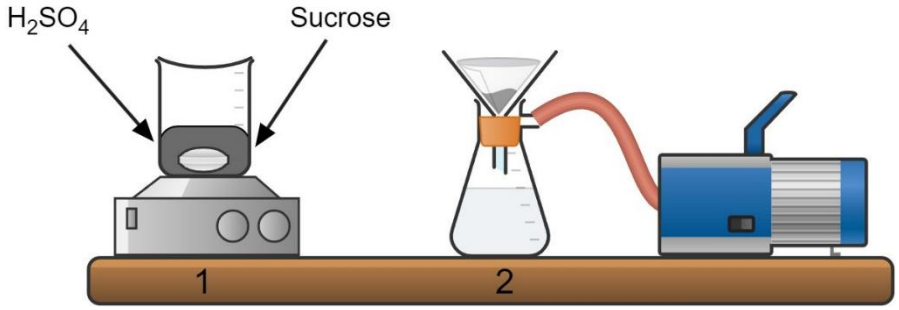

Figure 21 - Visual representation of the scheme utilized for the production and filtration of the hydrochar using Chemix Lab diagrams

The hydrochar samples were characterized using a comprehensive array of methods, including SEM-EDS, XRD, Raman Spectroscopy, TGA, and FTIR. The morphology and near-surface elemental composition of the hydrochar were analyzed using a Hitachi S-2400 Scanning Electron Microscope (SEM), equipped with an Energy Dispersive Spectrometer (EDS) and a Bruker SDD light element detector. Digital images were captured using Bruker Esprit 1.9 software at a resolution of 4 nm and an accelerating voltage of 25 kV. This high resolution enabled a detailed examination of the hydrochar surface structures, ensuring precise identification and mapping of elemental distributions. Phases within the hydrochar were elucidated using an X-ray diffractometer, specifically the Panalytical X'PERT PRO model. This analysis employed Cu Kα radiation and referenced the Powder Diffraction File™ database from the International Centre for Diffraction Data (ICDD). Measurements were meticulously set with a 2θ range from 5° to 70°, a step size of 0.033° 2θ, and scan times of either 75 or 150 seconds per step for extended duration runs. The X-ray generator operated at 35 mA current and 40 kV voltage. The high-resolution data acquisition and precise calibration ensured accurate phase identification and robust analytical results. Raman spectroscopy was utilized to evaluate the degree of graphitization in the hydrochar. Spectra were acquired using a LabRAM HR 800 Evolution confocal Raman microscope (HORIBA Scientific) with 532 nm wavelength (green light) radiation and a 50x visible objective. Spectral data were collected over a range from 2250 to 650 cm^{-1}. For accuracy and clarity, all Raman spectra underwent baseline correction and normalization before further deconvolution analysis.

Thermogravimetric analysis of the hydrochar samples was conducted using a NETZSCH STA 409 PC/PG system, which facilitates comprehensive thermal characterization by monitoring mass changes as a function of temperature. The thermal analysis covered a range from 30 to 1100°C with a heating rate of 30.0°C/min. The measurements were executed under controlled conditions, ensuring precise and reliable data on thermal stability and composition. The advanced calibration and high-resolution capabilities of the system provided detailed insights into the material's thermal behavior and decomposition characteristics. The surface functional groups of the hydrochar and its feedstocks were examined using Fourier Transform Infrared Spectroscopy. Post-reaction characterization of various hydrochars was also performed. Each spectrum was obtained in attenuated total reflectance (ATR) mode using a PerkinElmer Spectrum Two IR spectrometer, outfitted with a Pike ATR accessory featuring a ZnSe crystal. IR spectra were recorded within the wavenumber range of 4000 to 600 cm^{-1}, with a resolution of 4 cm^{-1} and 4 scans. The resulting spectra were treated using the Kubelka-Munk function. This thorough analysis enabled a comprehensive assessment of the chemical interactions and functional group modifications occurring on the hydrochar surfaces, due to the esterification reaction modifications.

3.2. ESTERIFICATION REACTION EXPERIMENTS

After the production of the hydrochar, all the pre-steps necessary to make the reaction are done since the otter product used is commercial and doesn't need any preparation. However, for the esterification reaction, several parameters must be taken into consideration. The reaction was conducted with the assembly of the reaction scheme, illustrated in Figure 22. This scheme involves a heating blanket under a round bottom flask of 500 mL, with 3 parallel nozzles, the lateral nozzles were the same size (19/26) and the middle nozzle (29/32). This flask copulated into a reflux column, and a thermocouple, on the left nozzle, to provide continuous control of the reaction temperature. It is also important to note that the round bottom flask has an orbital magnetic stirring bar, in the interior, to provide continuous stirring throughout the reaction, more precisely at 1100 rpm. The methanol utilized was mixed with oleic acid (90%) with a molar ratio of 12:1.

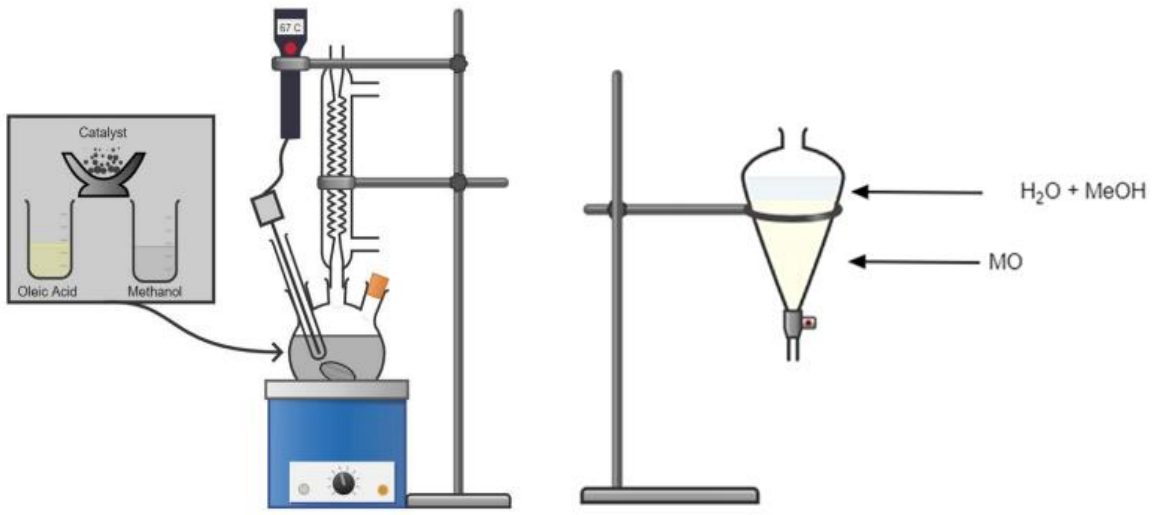

Figure 22 - Visual representation of the reaction scheme for the esterification and subsequently separation of the methyl oleate phase from the aqueous phase using Chemix Lab diagrams [adapted from [92])

With the arrangements of the scheme being made, the methanol (68.1g) and hydrochar (2.5g) were put into the bottom flask, for about 30 minutes. While this interaction was happening, the oleic acid was pre-heating at 70°C, and the reaction was being controlled at the methanol total reflux temperature of 67°C. After 30 minutes, the oleic acid was poured into the reaction flask, and the reaction progressed for 180 minutes. When the time was finished, the reaction mixture was subjected to a gravity filtration process, using a beaker glass and a paper filter (FILTER-LAB®) with pore apertures of 5-7 µm, to ensure the separation of the solid phase (hydrochar) and the liquid mixed phase. When the liquid phase was separated from the solid phase, it was then transferred to a settling funnel, to separate the different phases, more precisely, of the methyl oleate from the aqueous phase, and in certain cases from the methanol left from the reaction. Figure 22 demonstrates the separation of the different phases.

To ascertain the methyl oleate yield of samples synthesized under varying catalytic conditions, it was essential to establish a calibration curve. It is pertinent to mention that the methyl oleate utilized in the calibration process was derived from the conventional esterification of anhydrous oleic acid (99%) using a homogeneous catalyst (H_2SO_4). For this procedure, reference samples with varying MO yields were prepared by blending known quantities of MO with OA. In order for the calibration to be correct, the oleic acid needed to suffer a drying process, in this case by a Rotavapor® R-215. A sample of (200 mL) was placed in a round-bottomed flask and heated using a heating fluid in a water bath at 60°C under reduced pressure, at about 100 mmHg, for 30 minutes. After drying, the oleic acid was 99% pure, as confirmed by the FTIR method. Dried oleic acid, standard solutions were prepared for the construction of the calibration curve, which would be used to quantify the methyl oleate produced in the esterification reactions. After the drying step of the oleic acid, the absence of the broad band around 3400 cm^{-1}, in the FTIR spectrum confirmed an effective moisture removal. The resultant MO concentrations spanned a representative range of the produced samples, as illustrated in Figure 23.

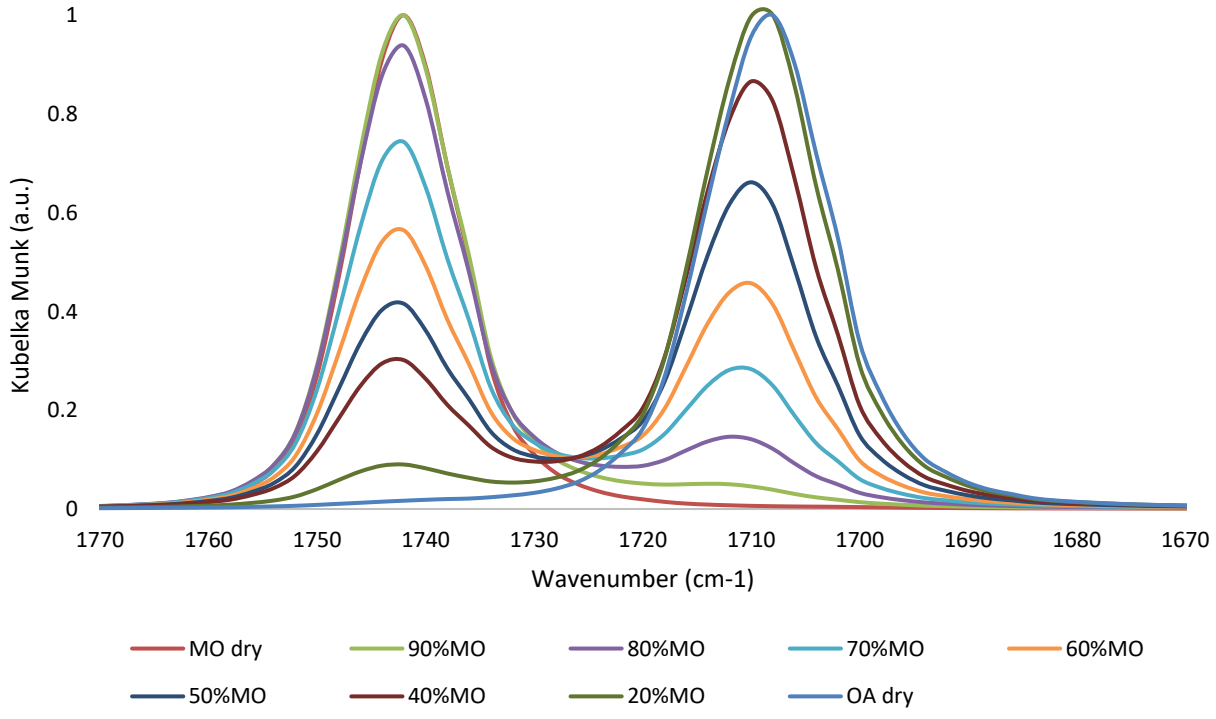

Figure 23 - FTIR spectrum of methyl oleate obtained for the calibration curve

The analysis of Figure 23 reveals a progressive enhancement in the absorbance band at 1742 cm^{-1}, indicative of the methyl ester content, corresponding to the decreasing oleic acid concentration and the increase in MO incorporation [102]. Conversely, the band at 1710 cm^{-1}, characteristic of oleic acid, decreased in intensity with rising MO content [103]. This inverse relationship between the peaks was needed for the development of the calibration curve depicted in Figure 24.

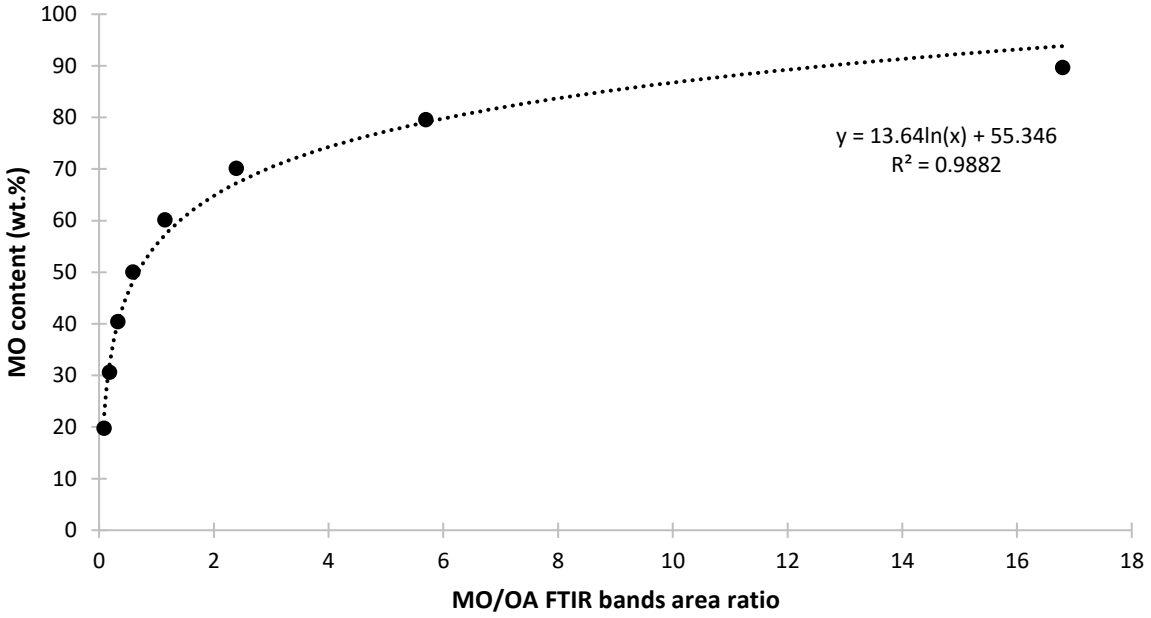

Figure 24 - Calibration curve for MO yield determination by area ratio of FTIR bands centered at 1742cm^{-1} (MO) and 1710cm^{-1} (OA)

Moreover, the calibration curve facilitated the quantitative analysis of MO in the experimental samples, thereby enabling the accurate assessment of catalytic efficiency. This method underscores the pivotal role of precise spectral analysis in the quantification of esterification products, contributing significantly to the optimization of catalytic processes. Furthermore, the findings elucidated the correlation between catalyst type and reaction conditions, thereby advancing the understanding of catalytic mechanisms in esterification reactions.

Values below 20% are deliberately excluded from the graph because they result in MO/OA ratios that are either negative or exceedingly close to zero. In such cases, the logarithmic function becomes problematic: it is undefined for negative values and exhibits an extremely steep incline for values just above zero. This steepness can introduce substantial variability and inaccuracies in data representation. By focusing on values above the 20% threshold, the logarithmic relationship between the MO/OA ratio and the percentage of MO remains stable and reliable. This approach enhances the clarity and precision of the understanding regarding the efficiency and yield of the process, as it avoids the distortions that arise from the unpredictable behavior of the logarithmic function at very low values.

4. RESULTS AND DISCUSSION

4.1. QUANTIFICATION OF METHYL OLEATE PERCENTAGE IN THE SAMPLES

To quantify the methyl oleate in the different samples produced, it was necessary to submit them to an FTIR analysis. Through that method the MO% was determined and synthesized in the following Figure 25. Table 12 illustrates the distinct molar and mass sulfonation ratios, and the type of feedstock used in each sample. It should be noted that for the esterification reaction, all the samples were subjected to a reaction molar ratio condition of 12:1 (methanol/ oleic acid).

Table 12 - Reactional conditions for distinct feedstocks for the production of hydrochar samples

Sample number	Feedstock	Molar sulfonation ratio	Mass sulfonation ratio
1	Cornstarch hydrochar (HC-C)	1:1	-
2		1:3	
3		1:5	
4	Sucrose hydrochar (HC-S)	1:1	-
5		1:3	
6		1:5	
7	Banana peel hydrochar (HC-BP)	-	1:1
8			2:1
9			3:1
10	Fructose hydrochar (HC-F)	1:1	-
11		1:3	
12		1:5	
13	Orange peel hydrochar (HC-OP)	-	1:1
14			2:1
15			3:1

From the observation of Figure 25, it was obvious that the highest MO content was found in the sample produced from HC-S with a molar sulfonation ratio of 1:1, while approximate values were found for the HC-OP with a mass sulfonation ratio of 2:1. The lowest content was observed at the HC-BP samples for mass sulfonation ratio of 1:1 and 3:1, indicating an optimal sulfonation ratio for that sample of 2:1.

Briefly, almost all the samples followed the same trend, with a higher methyl oleate percentage, related to a lower sulfonation ratio of the hydrochar samples. With some exceptions for the HC-OP (2:1), and all the cornstarch samples.

By comparison with literature values results (Dias et al 2024) it seems that the increase of the sulfonation ratio has been linked to an increase of MO%, which was not the case in this work, since the optimal values of the sulfonation ratio were varied, many times at 1:1 ratio, but sometimes also with a 2:1 ratio.

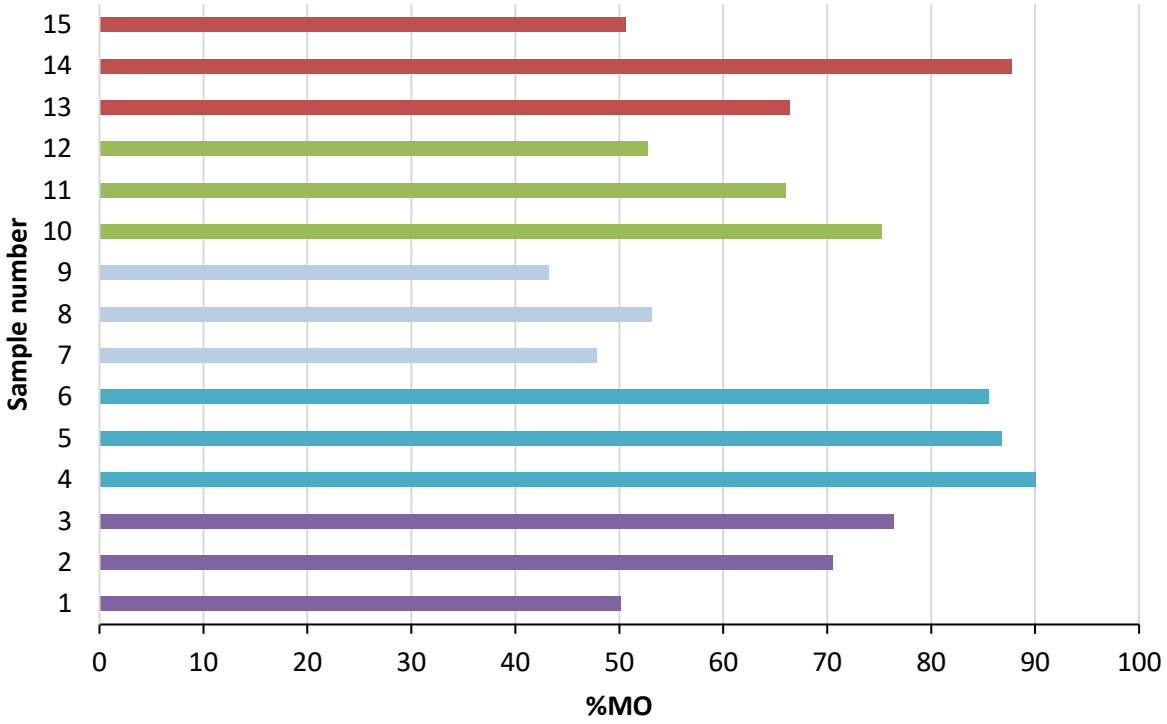

Figure 25 – Percentage of methyl oleate present in each sample, through distinct hydrochar samples

MO content was evaluated across 15 different samples produced with hydrochar samples derived from various feedstocks. Among the hydrochar samples, those derived from sucrose exhibited the highest production efficiencies. Sample 4, with a molar sulfonation ratio of 1:1, achieved a remarkable 90.1% MO yield, the highest across all tested samples. The hydrochar samples derived from cornstarch also showed significant production efficiencies. Sample 1, with a molar sulfonation ratio of 1:1, exhibited a lower MO yield of 50.2%, while samples 2 and 3, which were derived from cornstarch hydrochar (HC-C) with increasing sulfonation ratios of 1:3 and 1:5, achieved 70.6% and 76.4% MO production, respectively. Similarly, the hydrochar samples derived from fructose demonstrated moderate to high efficiencies. Sample 10, with a 1:1 molar sulfonation ratio, produced 75.3% MO, whereas samples 11 and 12, with sulfonation ratios of 1:3 and 1:5, exhibited lower efficiencies of 66.0% and 52.8%, respectively.

In the case of banana peel hydrochar (HC-BP), the results were more varied. Sample 7, with a 1:1 sulfonation ratio, produced 47.7% MO. However, when the sulfonation ratio was increased to 2:1 in sample 8, the MO yield improved slightly to 53.1%. Interestingly, further increasing the ratio to 3:1 in sample 9, resulting in a significant drop in efficiency, with only 43.2% MO produced. This suggests that beyond a certain threshold, higher sulfonation ratios may have a detrimental effect on the catalytic performance of banana peel hydrochar. Sample 13, with a 1:1 sulfonation ratio, exhibited a 66.5% MO yield.

This efficiency increased significantly to 87.8% in sample 14, where the sulfonation ratio was raised to 2:1, marking one of the highest MO yields observed among the hydrochar samples. However, a further increase in sulfonation ratio to 3:1 in sample 15 resulted in a substantial decrease in efficiency, with the MO yield dropping to 50.7%. Similar to the banana peel hydrochar, this suggests that excessively high sulfonation ratios may reduce the catalytic effectiveness of orange peel hydrochar. The following experimental analysis methods were only applied to the hydrochar samples with the best catalytic performance, in terms of the percentage of methyl oleate production. In this case, the HC-S (1:1), and HC-OP (2:1) samples. To have fully comparative data from samples, another sample was chosen to be characterized by different methods, in this case, a sample with a less appreciative performance, that was the case of the HC-BP (3:1) sample.

4.2. CHARACTERIZATION OF HYDROCHAR

4.2.1. XRD

Figure 26 presented below shows the X-ray diffraction patterns of hydrochar produced with sucrose (HC-S), banana peel (HC-BP), and orange peel (HC-OP). The graph displays two broad bands centered around 23° and 41°, which are attributable to the (002) and (001) graphitic planes, respectively [7]. These broad peaks suggest that the hydrochars possess amorphous structures, characterized by disordered sheets of polycyclic aromatic carbon compounds [7]. The low intensity of these peaks indicates a minimal content of crystalline graphite, highlighting the predominance of amorphous carbon over well-ordered graphitic structures [7]. The lack of well-defined peaks indicates that no discrete mineral phase was detected, except for the anhydrite crystals in the HC-OP [104]. Thus, the orange peel and banana peel have a completely amorphous structure, which is expected for organic materials [104].

In contrast, the HC-OP sample exhibits a fine and intense peak at $2\theta = 25.48^{o}$ and the others ($2\theta = 31.3°$, 36.17°, 38.6°, 40.8°, 43.42°, 48.7°, 52.3° and 55.7°) are mainly due to the presence of $CaSO_4$, meaning that hydrochar has also a crystalline structure [105]. Chemical constituents inherent to different types of residual biomass, such as orange or banana peels, can be responsible for the retention or formation of mineral species, such as arcanite (K_2SO_4) or anhydrite ($CaSO_4$) [106]. Additionally, the composition of the orange peel boosts the formation of this mineral, due to the significant percentage of calcium in its composition, approximately 161mg per 100g of peels, a value defined as quadruple the calcium content found in banana peels [107, 108].

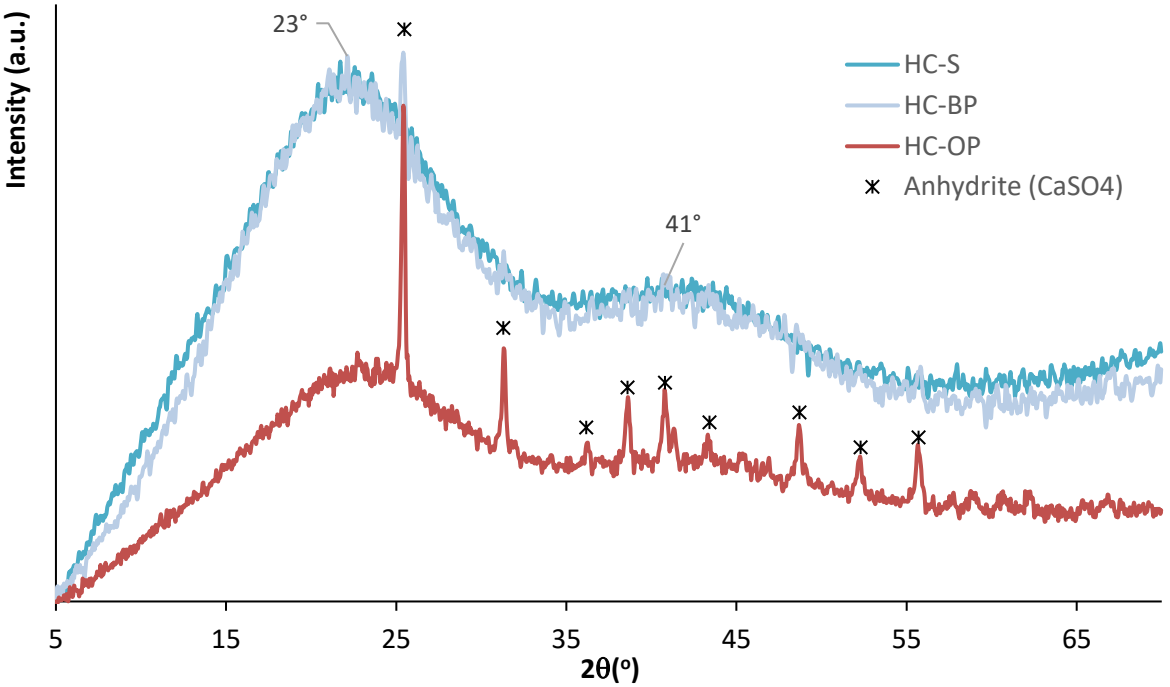

Figure 26 - X-ray diffraction patterns of HC-S (1:1), HC-BP (3:1), HC-OP (2:1) produced before the reaction

Regarding the diffractogram presented in Figure 27, the XRD spectrum of the catalysts studied after being subjected to esterification reactions, post reaction catalyst (PRC), reveals several key observations. Notably, the narrowing of the bands centered at 2θ = 20° indicates that the previously amorphous graphite, as characterized in Figure 27, has transitioned to a significantly more crystalline form [109]. Concerning the anhydrite crystals observed in the hydrochar sample derived from orange peels, all characteristic peaks remained unchanged in intensity, suggesting that the esterification process did not significantly alter the crystalline nature of this mineral within the sample.

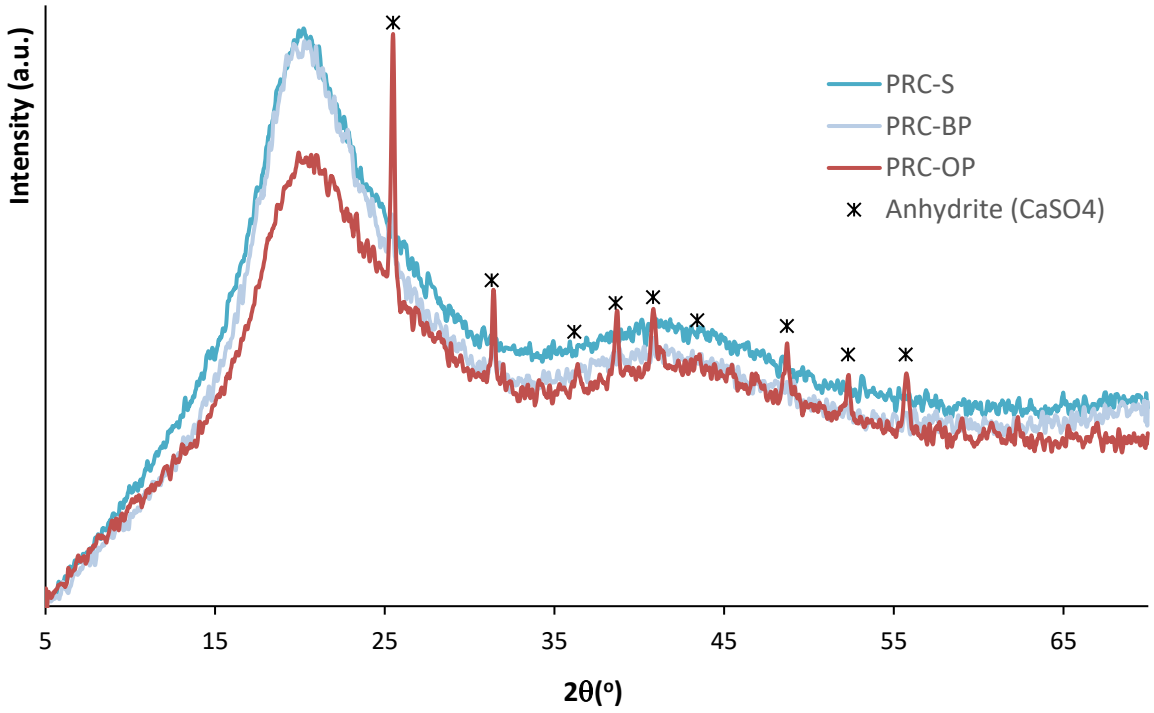

Figure 27 - X-ray diffraction patterns of PRC-S (1:1), PRC-BP (3:1), PRC-OP (2:1) after the esterification reaction

4.2.2. ATR-FTIR

FTIR was used to identify the functional groups present on the surface of the hydrochar samples (HC-S (1:1), HC-BP (3:1), HC-OP (2:1)), before the esterification reaction, as shown in Figure 28. A band was observed at 2976 cm^{-1} in all three samples, corresponding to the stretching vibration of hydroxyl (-OH) groups [110]. This indicates the presence of hydroxyl-containing compounds, such as alcohol, phenols, or water, either free or involved in hydrogen bonding [110]. The consistent appearance of this band suggests that hydroxyl groups are a common feature across the biomass-derived hydrochar samples, contributing to their hydrophilic nature [110]. In addition, a small but distinct peak was identified at 2172 cm^{-1}, which is attributed to the stretching vibration of silicon-hydrogen (-Si-H) bonds [111]. This indicates the presence of siliceous materials, possibly from inherent silica content in the biomass or contamination during sample processing [111]. The spectral region around 1774 cm^{-1} and 1700 cm^{-1} exhibited absorption bands characteristic of carboxylic acid groups, particularly associated with the carbonyl (C=O) stretching vibrations [112, 92].

These bands indicate that carboxylic acids or esters are present within the biochar matrix, implying that the thermal decomposition of biomass during hydrothermal carbonization did not completely eliminate oxygen-containing functional groups [112]. This residual oxygen content, reflected by the carbonyl bands, plays a crucial role in the surface chemistry and reactivity of the hydrochar [112].

Another carbonyl-related band was observed at 1460 cm^{-1}, further confirming the presence of various carbonyl-containing functional groups, such as ketones, aldehydes, and carboxylates [7]. A band at 1574 cm^{-1} was assigned to the stretching vibrations of carbon-carbon double bonds (-C=C), which are typically associated with aromatic rings [113]. This suggests the formation of polyaromatic structures during the hydrothermal carbonization process, contributing to the stability and carbon-rich nature of the hydrochar [113]. The presence of aromatic rings also indicates significant aromatic condensation, a process that enhances the structural integrity and potential adsorption capacity of the biochar [113].

The analysis also identified a band at 1144 cm^{-1}, corresponding to the stretching vibrations of hydroxyl-carbon (-C-OH) groups [112]. This band showed a progressive increase in intensity, particularly in the fruit peel-derived biochar samples (HC-OP and HC-BP), suggesting a higher content of hydroxyl-functionalized organic compounds in these samples [112]. In the spectral region between 1050 and 1010 cm^{-1}, three consecutive peaks were reported. All three peaks were associated with SO_2 asymmetric vibrations, indicating that the sulfonation process introduced sulfonated groups in all the hydrochar samples [114]. Another SO_2 vibration was seen at 590 cm^{-1}, underscoring the effectiveness of introduction, of sulfonated groups in the hydrochar samples [114]. The presence of sulfonate groups (-SO_2) could enhance the catalytic or adsorptive properties of the biochar, broadening its potential applications [113].

A distinct band at 672 cm^{-1} was identified as being associated with calcium-related vibrations [115]. This band was most prominent in the HC-OP sample, reflecting the high calcium content in orange peel biomass. The presence of calcium could influence the structural properties and, consequently, the applications of the resulting hydrochar sample, favoring the use for soil amendment and removal of pollutants. [115, 116]. Finally, a subtle band at 516 cm^{-1} was observed, indicative of calcium oxide (-Ca-O) stretching vibrations linked to monoclinic phase of CaO nanoparticles in the sample, also, the high content of calcium in orange peel samples, can be a factor that confirms the presence of the (-Ca-O) peak in this HC-OP sample spectrum. [116,117].

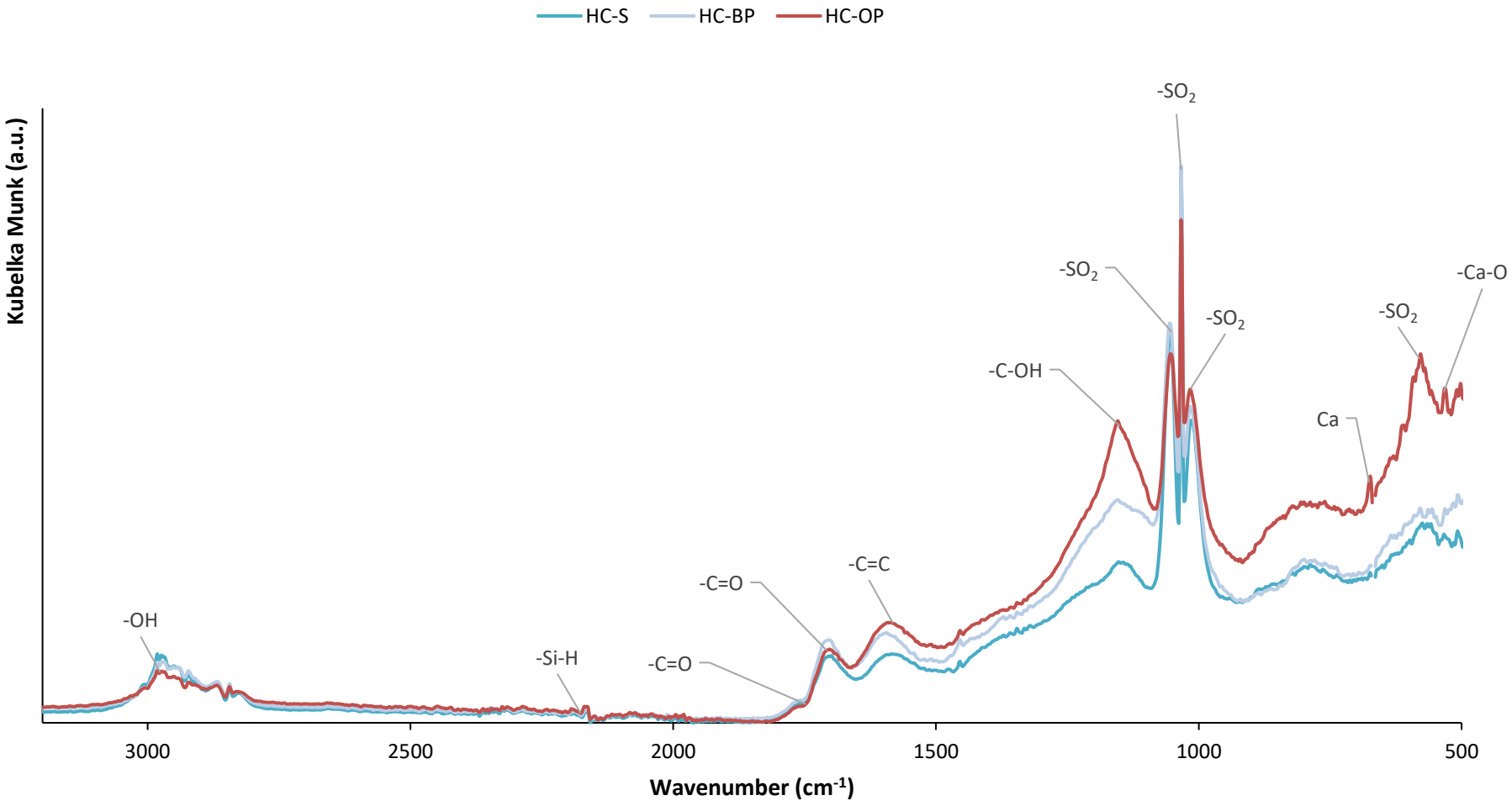

Figure 28 - FTIR analysis to identify functional groups on the surface of the catalysts before the esterification reaction: HC-S (1:1), HC-BP (3:1), HC-OP (2:1)

ATR-FTIR analysis of the catalysts post-reaction (Figure 29) provided significant insights into the chemical transformations and functional groups present. A distinct vibrational peak observed at 3022 cm^{-1} is indicative of the presence of characteristic (-C-H) bonds, which are typically associated with organic compounds [118]. Additionally, the spectral peaks identified at 2922 cm^{-1} and 2855 cm^{-1} correspond to aliphatic (-C-H) stretching vibrations specifically related to alkenes, further elucidating the structural composition of the catalysts [119].

Significantly, three prominent (-C=O) stretching vibrations were detected at 1742 cm^{-1} and 1712 cm^{-1}, which are likely attributable to carbonyl functional groups, with the 1742 cm^{-1} being related to the esters formed during the reaction, and the band centered at 1712 cm^{-1} corresponding to the oleic acid typical band [120,121]. These carbonyl groups are believed to have originated from esters formed during the esterification reactions, highlighting the chemical evolution that the catalysts undergo during the process [120].

Moreover, a further (-C=O) stretching vibration was evident at 1653 cm^{-1}, which can be associated with amide functionalities, providing an indication of the complex interplay of chemical groups within the catalytic structure [122]. The presence of aromatic (-COOH) groups was clearly discerned at 1456 cm^{-1}, underscoring the abundance of oxygenated functional groups within the biochar component of the catalyst [123]. This finding is particularly significant as it suggests that the biochar, a crucial component, contributes to catalytic activity through its rich oxygenated functionality [123].

Additionally, at 1436 cm^{-1} and 1050 cm^{-1}, the data revealed an aromatic vibration, which was intricately coupled with (-C-H) and (-C-O) stretching vibrations originating from carbohydrates [124]. This observation further reinforces the complex nature of the catalysts, where carbohydrate-derived structures play a role [124].

Within the spectral range of 1276 cm^{-1} to 1192 cm^{-1}, several distinct peaks were identified, each corresponding to various functional groups, including hydroxyl groups, aromatic (-C-O) stretches, and (-C-O) secondary alcohol stretches [125, 126, 127]. These findings indicate diverse chemical interactions and modifications occurring within the catalyst during the reaction process [127]. Notably, a characteristic absorption band at 1166 cm^{-1}, which is typically associated with lignin biomass, was observed [128]. This band is linked to (-C-O-C) stretching vibrations in esters, which were produced as a result of the esterification reaction, emphasizing the chemical environment within the catalyst [128].

Furthermore, additional peaks observed at 1121 cm^{-1} and 595 cm^{-1} were attributed to (-C-O) stretching vibrations of carbohydrates and (-OH) vibrations, respectively [128, 129]. These peaks provide further evidence of the intricate chemical structure and the presence of various functional groups within the catalyst [128]. Lastly, the peak identified at 720 cm^{-1} is suggestive of CH2 wagging, a vibration characteristic of long-chain alkanes, indicating the presence of extended hydrocarbon chains within the catalyst matrix [130].

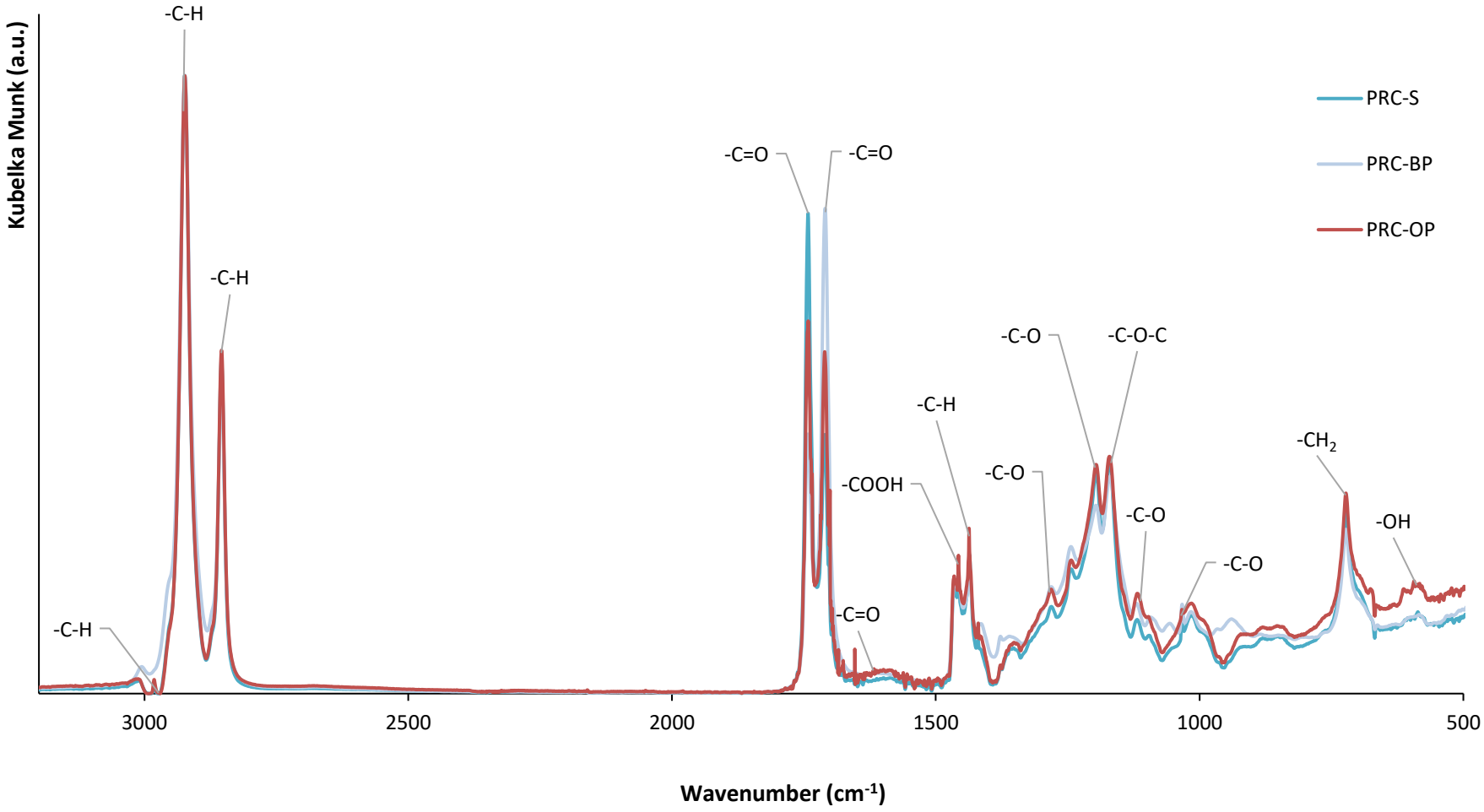

Figure 29 - FTIR analysis to identify functional groups on the surface of the catalysts after the esterification reaction: PRC-S (1:1), PRC-BP (3:1), PRC-OP (2:1)

4.2.3. RAMAN

The Raman absorption spectra acquired in the range of 800-1900 cm^{-1} were curve-fitted to gain insights into the structural features of HC-BP, HC-S, and HC-OP. Each Raman spectrum was deconvoluted into six Gaussian bands with a specific identification according to the position of the band in the spectrum. Table 13 identifies the bands that compose each spectrum with the according nomenclature.

Table 13 - Gaussian bands characterization adapted from [131]

Band	Band position (cm^{-1})	Hybridized orbital
S_L	1230-1262 [132]	sp^2, sp^3 [132]
D	1365-1370 [7]	sp^2 [132]
G	1580-1596 [7]	sp^2[132]
Valley	≃1500 [133]	sp^2, sp^3 [131]
G_L	1700-1740 [133]	sp^2 [132]

The S_L band, located at 1230-1262 cm^{-1} was correlated with the cross-linking structures such as aryl-alkyl ethers [132]. The D band, attributed to sp^2 vibrations of species with defects, is located between 1365-1370 cm^{-1} and is one of the main bands that is analyzed to evaluate the degree of defects within the structure of the hydrochars produced, reflecting the extent lattice of imperfections and surface defects [7]. The increased presence of surface defects and higher overall defectiveness boosts the number of active sites for the sulfonating agent and improves the interaction between the agent and the material surface, providing better catalytic characteristics for the sample [134].

The G band, attributed to the sp^2 vibrations of the graphitized species, located between 1580-1596 cm^{-1} indicates the presence of nanocrystalline graphite, which suggests that the samples exhibit a structure of aggregated carbon, dispersed within the amorphous carbon matrix [7]. The G peak is observed in all graphic structures due to its association with the quadrant breathing modes of aromatic rings and E_{2g}^2 vibration mode of the hexagonal lattice in graphite [7].

Between the D and G bands is the valley band, approximately centered at 1500 cm^{-1}, and corresponds to what has been attributed mainly to the semicircular breathing of aromatic rings and/or typical structures in amorphous carbon, such as the small degree of polymerization of aromatic rings (system of 3-5 polymerized aromatic rings) [7,133]. Finally, the G_L band located between 1700 and 1740 cm^{-1} represents the absorption band of a (-C=O) carbonyl structure in hydrocarbons [133] Figure 30 to 32 demonstrates the Raman spectra of the different hydrochar samples.

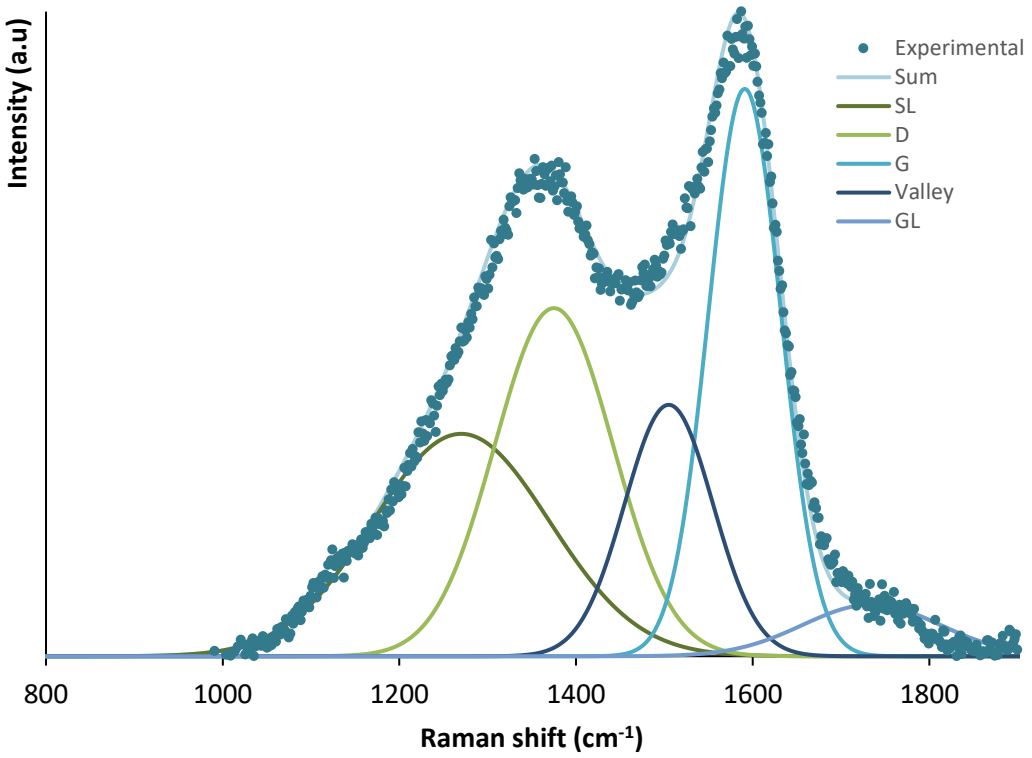

Figure 30 - Raman spectrum before the esterification reaction: HC-BP (3:1)

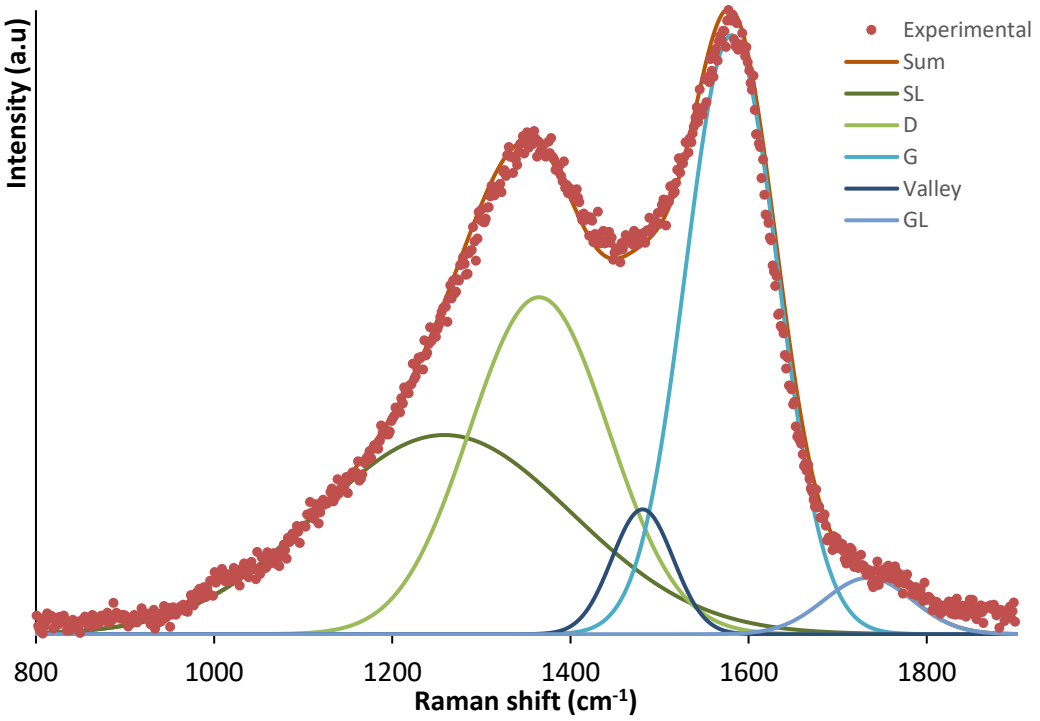

Figure 31 - Raman spectrum before the esterification reaction: HC-OP (2:1)

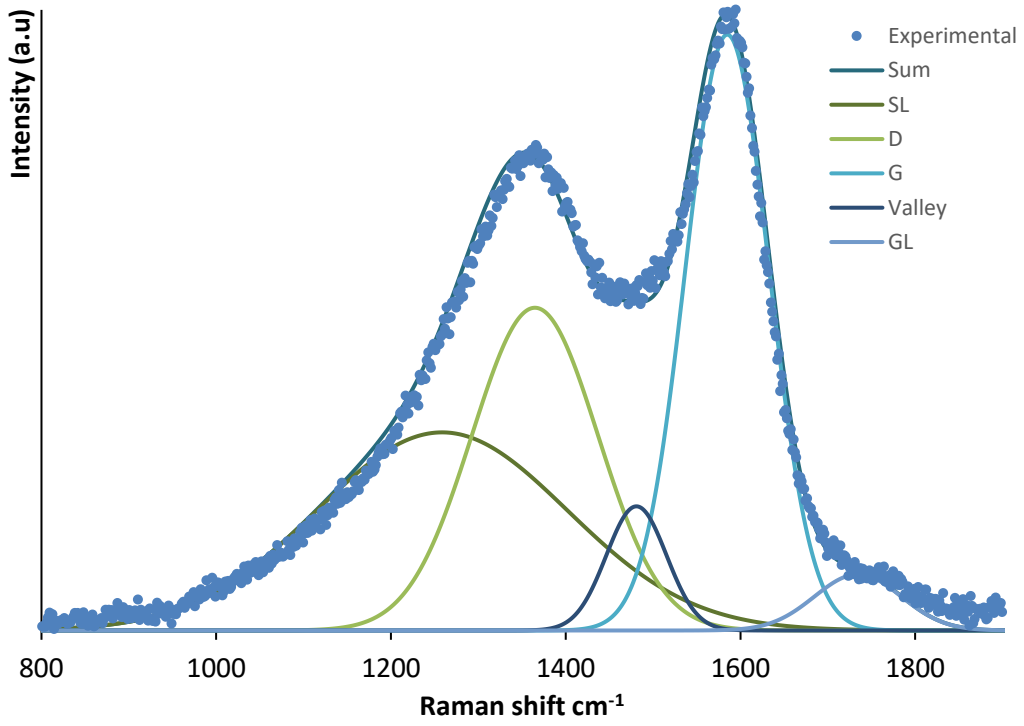

Figure 32 - Raman spectrum before the esterification reaction: HC-S (1:1)

For the same samples, presented in Table 14 it is observed the intensity of the D band, G band, and the ID/IG ratio, which relates the disorder induced by the D band with the graphite levels of the G band [135]. A lower I(D)/I(G) indicates a higher degree of graphitization due to the restructuring of the carbon atoms, and the formation of larger graphitic segments, that reduce the number of defects [114].

Table 14 - Identification of the intensity of D and G band and corresponding ratio between for each sample

		HC-BP	HC-S	HC-OP
D band	Wavenumber (cm^{-1})	1375	1364	1364
	ID	94.8	108.2	105.6
G band	Wavenumber (cm^{-1})	1591	1585	1581
	IG	90.4	115.5	132.3
ID/IG		1.05	0.94	0.79

For the D band, the wavenumbers are similar across all samples, with HC-BP at 1375 cm^{-1} and both HC-S and HC-OP at 1364 cm^{-1}, indicating a comparable level of structural disorder. The intensity of the D band (ID) varies, with HC-S exhibiting the highest at 108.2, followed by HC-OP at 105.6, and HC-BP at 94.8. A higher D band intensity typically reflects a greater degree of disorder in the carbon structure [7]. The G band wavenumbers also show minimal variation, ranging from 1581 cm^{-1} in HC-OP to 1591 cm^{-1} in HC-BP. The intensity of the G band (IG) increases progressively from HC-BP (90.4) to HC-OP (132.3), with HC-S at 115.5, suggesting that HC-OP has the most graphitic character among the samples [7]. The ID/IG ratio indicates that the degree of disorder in the carbon material is highest for HC-BP (1.05), suggesting that it has the most disordered structure [135]. HC-S has a slightly lower ratio of 0.94, indicating a moderate disorder, while HC-OP has the lowest ratio of 0.79, implying the most ordered structure.

4.2.4. TGA

The thermogravimetric analysis and respective profiles of the three hydrochar samples present in Figure 33 revealed a complex and distinct thermal degradation behavior, reflective of compositional matrices and structural characteristics. These curves, which delineate the residual mass percentage as a function of temperature, provide crucial insights into the thermal stability and degradation mechanisms of the hydrochar samples [136]. The Figure relates the thermograms mass loss curve (TG) and the rate of mass loss (DTG) of the hydrochar samples, from 30 to 1100 °C.

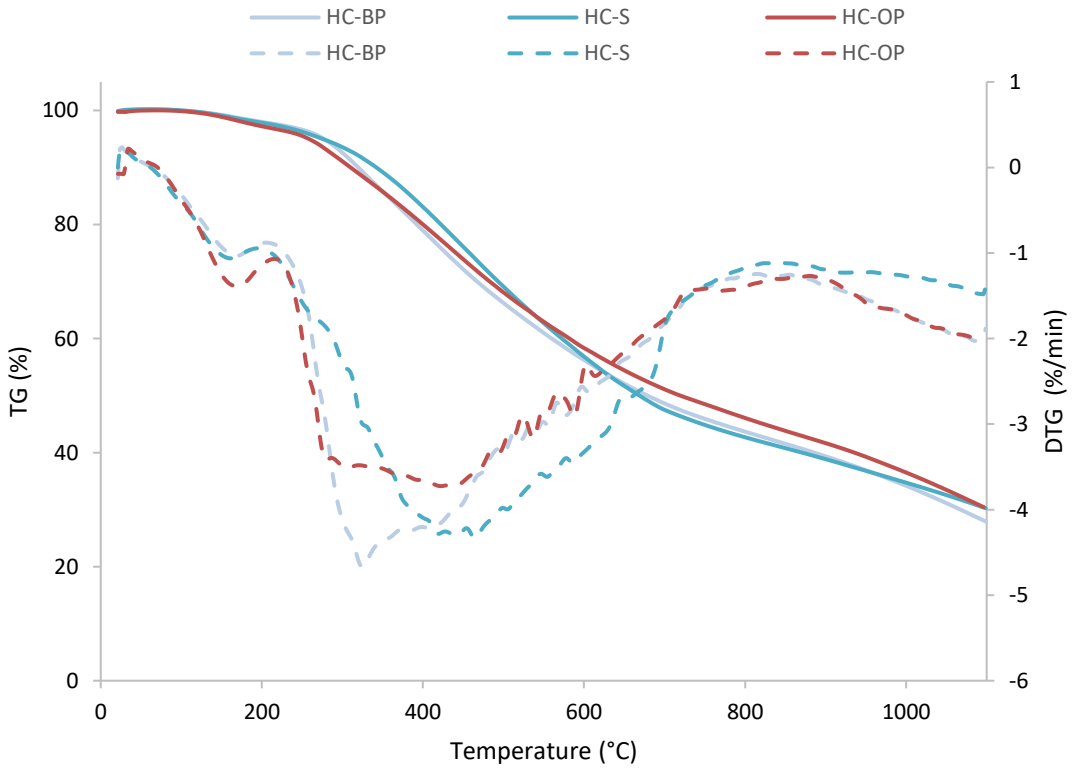

Figure 33 - TG analysis to identify the thermo profiles of the catalysts before the esterification reaction: HC-S (1:1), HC-BP (3:1), HC-OP (2:1)

The HC-BP sample exhibits an early onset of significant mass loss, initiating around 100°C. This initial mass reduction is likely attributable to the evaporation of physically adsorbed moisture and low-molecular-weight volatile compounds, which are abundant in lignocellulosic materials like banana peel [136].

As the temperature increases, HC-BP undergoes a pronounced multi-stage weight loss between 200°C and 400°C. This can be correlated with the sequential decomposition of hemicellulose, cellulose, and lignin, which are the primary constituents of lignocellulosic biomass [137]. In contrast, the HC-S sample exhibits a more uniform and gradual mass loss curve, while the degradation onset for HC-S, occurs at a relatively higher temperature, which suggests a different thermal stability profile, with the absence of distinct mass loss stages, as observed in HC-BP. The mass loss for HC-OP initiates post 200°C and proceeds gradually, suggesting a less complex degradation spectrum compared to HC-BP.

The dashed line sample curves offer a more nuanced understanding of the decomposition kinetics by representing the rate of mass loss as a function of temperature. The presented HC-BP sample with a dashed line in Figure 33 is characterized by distinct peaks, reflective of its multi-phasic degradation process. The most prominent peak occurs around 300°C, corresponding to the thermal decomposition of cellulose, a primary constituent of lignocellulosic biomass [137]. The presence of multiple peaks underscores the heterogeneity of the HC-BP hydrochar, with each peak representing the degradation of different components such as hemicellulose and lignin, each with its distinct thermal degradation temperature [137].

In contrast, the dashed line curve of HC-S is marked by a broader, less distinct peak centered around 350°C. This broad peak suggests a more homogeneous material undergoing decomposition in a relatively uniform manner, which aligns with the simpler, non-lignocellulosic composition of sucrose hydrochar, with the sample weight beginning to decrease with an increase of the decomposition rate due to the exothermic pyrolysis [138].

The dashed line curve of HC-OP also exhibits distinct peaks, albeit with a thermal degradation profile that slightly deviates from HC-BP. The primary peak around 320°C suggests a decomposition pathway influenced by the specific chemical composition of orange peel, which, while containing lignocellulosic components, likely possesses a unique distribution of pyrolysis-sensitive compounds [136].

4.2.5. SEM-EDS

To gain a more profound understanding of the morphological characteristics of the hydrochar samples, as previously mentioned, SEM analysis was conducted for each specimen at a magnification of 160x. Figure 34 presents the surface topography of the samples, before and after reaction, with imaging performed under an accelerating voltage of 15.0 kV, utilizing a secondary electron detector (SED) [139]. The microstructural details observed through SEM provide insights into the texture, porosity, and surface heterogeneity of the hydrochar and post reaction hydrochar samples, with the column on the left, at Figure 34, resembling the hydrochar samples before reaction, and the right column presenting the post reaction catalysts morphology.

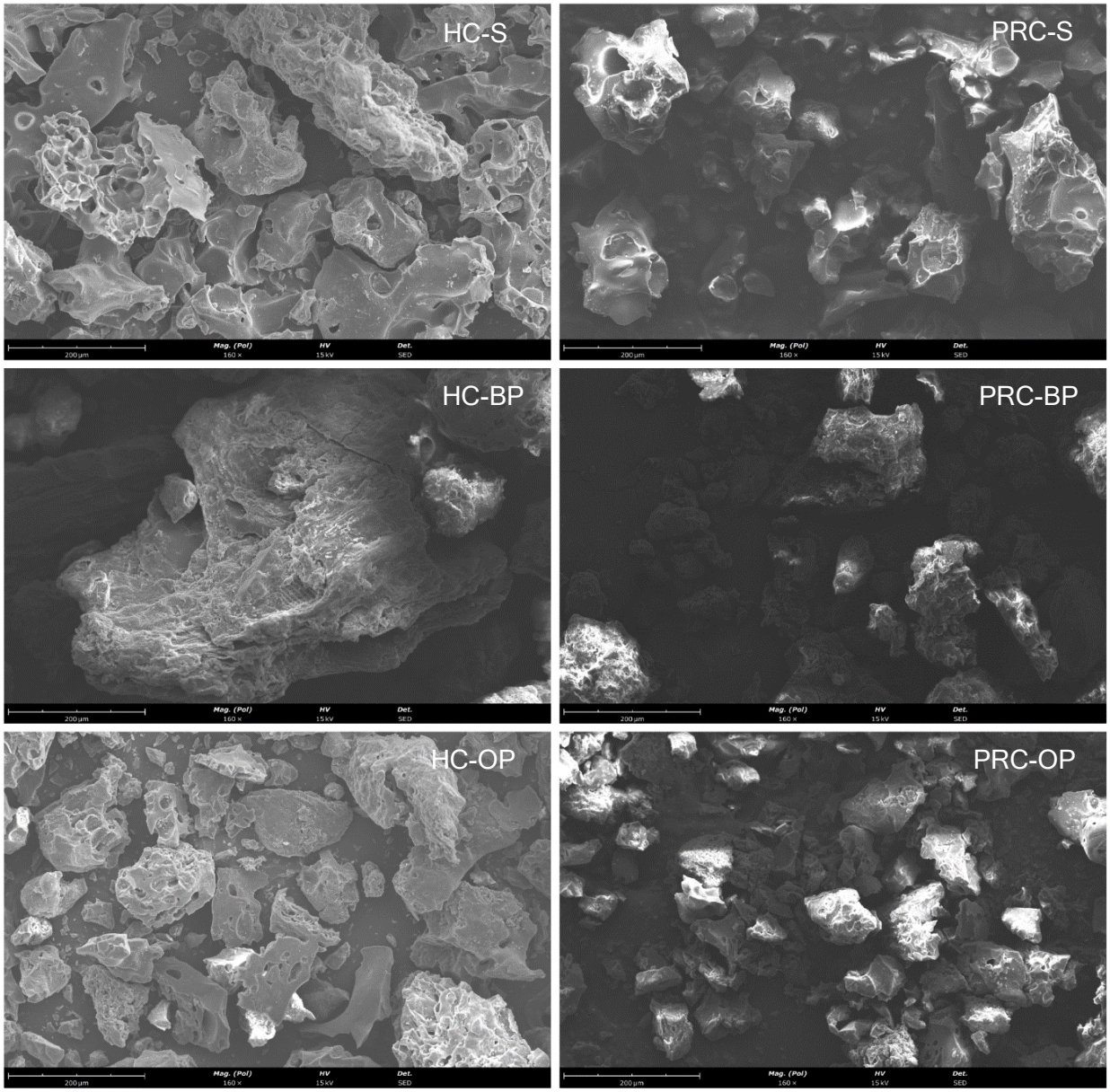

Figure 34 - SEM analysis to identify the morphology of the catalysts before the esterification reaction: HC-S (1:1), HC-BP (3:1), HC-OP (2:1) and after the reaction: PRC-S (1:1), PRC-BP (3:1), PRC-OP (2:1)

The SEM images of the fresh hydrochar samples reveal distinct surface morphologies across the three feedstocks. The HC-S sample displays a highly porous structure, characterized by irregularly shaped, and fragmented particles, with large cavities and rough surfaces. In contrast, the HC-BP sample shows a more compact and relatively smoother surface, with fewer large pores and visible cracks and fissures, indicating a more cohesive material. Lastly, the HC-OP sample exhibits a finer, more uniformly porous structure, with smaller and more evenly distributed pores. Table 15 enumerates the different inorganic components in the samples, before and after reaction, and the respective carbon and oxygen content, as the corresponding O/C atomic ratio. As illustrated in Table 15, the sulfur content for all the hydrochar samples shows that the process of sulfur insertion was effective, with a lower content (up to 5.13%) for the HC-S (1:1) and a gradual increase of S content to values of 6.01% and 7.11%, for the HC-BP (2:1) and HC-OP (3:1).

Table 15 - EDS analysis to identify the carbon and oxygen content of the catalysts, before the esterification reaction, and the respective inorganic elements

Element symbol	Samples					
	Sucrose		Orange peel		Banana peel	
	HC (1:1)	PRC	HC (2:1)	PRC	HC (3:1)	PRC
C	74.10	76.57	72.62	71.71	70.00	76.20
O	20.77	21.49	15.80	26.12	21.71	21.97
Si	-	-	-	-	1.53	0.32
S	5.13	1.94	7.11	1.38	6.01	1.51
Ca	-	-	4.47	0.79	-	-
K	-	-	-	-	0.75	-
Atomic ratio O/C	0.28	0.28	0.22	0.36	0.31	0.29

The calcium concentration in the HC-OP sample aligns with the findings from the FTIR analysis, which confirmed the presence of calcium-related functional groups, further corroborated by the XRD results, which identified the presence of calcium sulfate peaks. The potassium content was only found in the HC-BP, mostly related to its high content in banana peels, the biomass used for the production of this hydrochar sample [140]. Silica concentration was also only evidenced in the HC-BP, in small concentrations, as previously seen by the FTIR analysis, and mostly related to its nature presence in the banana peels [141]. The atomic ratio between O/C did not follow a specific pattern, in accordance with the sulfonation ratio, with the higher value being related to the sample that produced the lowest MO% content, and the two lower values of 0.28 and 0.22, related to the HC-OP and HC-S, respectively. These results suggest that lower atomic ratios between oxygen and carbon, with considerable concentrations of sulfur, produce better results, in terms of methyl oleate production.

5. CONCLUSIONS

This study demonstrated the effectiveness of hydrochar catalysts derived from agricultural waste in the esterification of oleic acid with methanol, highlighting their potential in sustainable biodiesel production. Among the tested catalysts, sucrose-derived hydrochar at a 1:1 molar sulfonation ratio achieved the highest methyl oleate yield of 90.1%. Close to this, orange peel-derived hydrochar at a 2:1 mass sulfonation ratio produced a significant yield of 87.8%. These results underline the superior performance of these feedstocks when the sulfonation and reaction conditions are optimized.

In contrast, the worst catalytic performance was observed with banana peel hydrochar at a 3:1 mass sulfonation ratio, where the MO yield dropped to 43.2%. These findings suggest that the efficiency of the catalysts is highly dependent on both the biomass source and the sulfonation ratio, with inappropriate ratios leading to reduced catalytic activity.

The catalysts were rigorously characterized using several techniques. X-ray diffraction (XRD) confirmed the presence of amorphous structures with some crystalline phases, especially in the orange peel hydrochar, which showed distinct peaks due to the presence of calcium sulfate ($CaSO_4$). Raman spectroscopy revealed the degree of graphitization, while FTIR analysis confirmed the presence of methyl ester peaks at 1742 cm^{-1}, indicating successful ester formation. Thermogravimetric analysis (TGA) showed that the hydrochar catalysts were thermally stable up to 1100°C, making them suitable for high-temperature applications.

The esterification reactions were conducted at a controlled temperature of 67°C under methanol reflux conditions, ensuring that the reaction environment remained consistent across all tests. The molar ratio of methanol to oleic acid was maintained at 12:1 for optimal reaction kinetics. The superior yield from sucrose and orange peel hydrochars reflects their enhanced surface properties and catalytic activity under these conditions.

Overall, this study demonstrates that hydrochar catalysts derived from renewable waste materials, particularly sucrose and orange peels, can significantly enhance biodiesel production. Optimizing the sulfonation ratio and reaction conditions is critical for maximizing yields. These results highlight the potential for scalable biodiesel production using cost-effective, sustainable catalysts, contributing to cleaner energy alternatives.

6. REFERENCES

[1] Subramaniam, Y., Masron, T., 2021. The impact of economic globalization on biofuel in developing countries. Energy Conversion and Management. Volume 10. 100064. https://doi.org/10.1016/j.ecmx.2020.100064

[2] Ali, K., Ahmad, M., Yusup, Y., 2020. Issues, Impacts, and Mitigations of Carbon Dioxide Emissions in the Building Sector. Sustainability. Volume 12. Issue 18. https://doi.org/10.3390/su12187427

[3] IEA (2024), CO2 Emissions in 2023, IEA, Paris. https://www.iea.org/reports/co2-emissions-in-2023. Licence: CC BY 4.0. Acessed 1 May 2024.

[4] Liu, Z., Deng, Z., Davis, S., Ciais, P., 2024. Global carbon emissions in 2023. Nature Reviews Earth Environment. Pages 253-254. https://doi.org/10.1038/s43017-024-00532-2

[5] Suhara, A., Karyadi., Herawan, SG., Tirta, A., Idris, M., Roslan, M., Putra, N., Hananto, A., Veza, I., 2024. Biodiesel Sustainability: Review of Progress and Challenges of Biodiesel as Sustainable Biofuel. Clean Technologies. Volume 6. Pages 886-906. Issue 3. https://doi.org/10.3390/cleantechnol6030045

[6] Yusuf, I., Flagiello, F., Ward, N., García, H., Rossa, C., Sotelo, M., 2020. Valorisation of banana peels by hydrothermal carbonisation: Potential use of the hydrochar and liquid by-product for water purification and energy conversion. Bioresource Technology Reports. Volume 12. 100582. https://doi.org/10.1016/j.biteb.2020.100582

[7] Dias, A., Pedra, I., Salvador, É., Rijo, B., Pereira, M., Serralha, F., Nogueira, I., 2024. Biodiesel Production over Banana Peel Biochar as a Sustainable Catalyst. Catalysts. Volume 14. Issue 4. https://doi.org/10.3390/catal14040266

[8] Tibolla, H., Pelissari, F., Martins, J., Vicente, A., Menegalli, F., 2018. Cellulose nanofibers produced from banana peel by chemical and mechanical treatments: Characterization and cytotoxicity assessment. Food Hydrocolloids. Volume 75.Pages 192-2018. https://doi.org/10.1016/j.foodhyd.2017.08.027

[9] Sanchez, M., Alzate, C., Toro, J., 2024. Orange Peel Waste as a Source of Bioactive Compounds and Valuable Products: Insights Based on Chemical Composition and Biorefining. Biomass. Volume 4. Pages 107-131. Issue 1. https://doi.org/10.3390/biomass4010006

[10] Bicu, I., Mustata, F., 2011. Cellulose extraction from orange peel using sulfite digestion reagentes.Bioresource Technology. Volume 102. Pages 10013-10019. Issue 21. https://doi.org/10.1016/j.biortech.2011.08.041

[11] Cavali, M., Junior, N., Sena, J., Woiciechowski, A., Soccol, C., Filho, P., Bayard, R., Benbelkacem, H., Junior, A., 2023. A review on hydrothermal carbonization of potential biomass wastes, characterization and environmental applications of hydrochar, and biorefinery perspectives of the process. Science of The Total Environment. Volume 857. Part 3. 159627. https://doi.org/10.1016/j.scitotenv.2022.159627

[12] Clarivate Web of Science, Copyright Clarivate 2024. All rights reserved. https://www.webofscience.com/wos/woscc/basic-search - Accessed 1 May 2024.

[13] Kumar, S., Soomro, S., Harijan, K., Uqaili, M., Kumar, L., 2023. Advancements of Biochar-Based Catalyst for Improved Production of Biodiesel: A Comprehensive Review. Energies. Volume 16. Issue 2. https://doi.org/10.3390/en16020644

[14] Ojewumi, M., Chen, G., 2024. Hydrochar Production by Hydrothermal Carbonization: Microwave versus Supercritical Water Treatment. Biomass. Volume 4. Pages 574-598. Issue 2. https://doi.org/10.3390/biomass4020031

[15] Masoumi, S., Borugadda, V., Nanda, S., Dalai, A., 2021. Hydrochar: A Review on Its Production Technologies and Applications. Catalysts. Volume 11. Issue 8. https://doi.org/10.3390/catal11080939

[16] Liu, Q., Kong, G., Zhang, G., Cao, T., Wang, K., Zhang, X., Han, L., 2023. Recent advances in hydrothermal liquefaction of manure wastes into value-added products. Energy Conversion and Management. Volume 292. 117392. https://doi.org/10.1016/j.enconman.2023.117392

[17] Khosravi, A., Zheng, H., Liu, Q., Hashemi, M., Tang, Y., Xing, B., 2022. Production and characterization of hydrochars and their application in soil improvement and environmental remediation. Chemical Engineering Journal. Volume 430. Part 4. 133142. https://doi.org/10.1016/j.cej.2021.133142

[18] Liu, Y., Sohi, S., Jing, F., Chen, J., 2019. Oxidative ageing induces change in the functionality of biochar and hydrochar: Mechanistic insights from sorption of atrazine. Environmental Pollution. Volume 249. Pages 1002-1010. https://doi.org/10.1016/j.envpol.2019.03.035

[19] Moszczyński, P., Tabarowski, Z., 2018. Chapter 32 - Meal Plans for Diabetics: Caloric Intake, Calorie Counting, and Glycemic Index. Nutritional and Therapeutic Interventions for Diabetes and Metabolic Syndrome (Second Edition). Pages 403-427. https://doi.org/10.1016/B978-0-12-812019-4.00032-5

[20] Niaz, K., Khan, F., Shah, M., 2020. Analysis of carbohydrates (monosaccharides, polysaccharides). DOI: 10.1016/B978-0-12-816455-6.00018-4

[21] Suárez, V., Ayuso, J., Rodríguez, A., Campo, D., Flórez, L., Aguilera, J., 2022. The Burden of Carbohydrates in Health and Disease. Nutrients. Volume 14. Issue 18. https://doi.org/10.3390/nu14183809

[22] Thota, S., Bag, P., Vadlani, P., Belliraj, S., 2022. Engineered Science Plant Biomass Derived Multidimensional Nanostructured Materials: A Green Alternative for Energy Storage. Engineered Science. Pages 31-58. DOI: 10.30919/es8d664

[23] Wyman, C., Decker, S., Himmel, M., Brady, J., Skopec, C., Viikari, L., 2005. Hydrolysis of cellulose and hemicellulose. Volume 1. Pages 1023-1062. DOI: 1:1023-1062 - SUBS - https://www.researchgate.net/publication/303131858_Hydrolysis_of_cellulose_and_hemicellulose

[24] Perez, D., Mayanga, P., Abaide, E., Zabot, G., Castilhos, F., 2022. Hydrothermal carbonization and Liquefaction: differences, progress, challenges, and opportunities. Bioresource Technology. Volume 343. 126084. https://doi.org/10.1016/j.biortech.2021.126084

[25] Ruiz, H., Galbe, M., Garrote, G., Gutierrez, D., Ximenes, E., Sun, S., Perez, D., Jasso, R., Sun, R., Yang, B., Ladisch, M., 2021. Severity factor kinetic model as a strategic parameter of hydrothermal processing (steam explosion and liquid hot water) for biomass fractionation under biorefinery concept. Bioresource Technology. Volume 342. 125961. https://doi.org/10.1016/j.biortech.2021.125961

[26] Sivaramakrishnan, R., Incharoensakdi, A., 2018. Microalgae as feedstock for biodiesel production under ultrasound treatment – A review. Bioresource Technology.Volume 250. Pages 877-887. https://doi.org/10.1016/j.biortech.2017.11.095

[27] Xia, C., Pathy, A., Paramasivan, B., Ganeshan, P., Dhamodharan, K., Juneja, A., Kumar, D., Brindhadevi, K., Kim, S., Rajendran, K., 2022. Comparative study of pyrolysis and hydrothermal liquefaction of microalgal species: Analysis of product yields with reaction temperature. Fuel. Volume 311. 121932. https://doi.org/10.1016/j.fuel.2021.121932

[28] Amalina,F., Razak, A., Krishnan, S., Sulaiman, H., Zularisam, A., Nasrullah, M., 2022. Biochar production techniques utilizing biomass waste-derived materials and environmental applications – A review. Journal of Hazardous Materials Advances. Volume 7. 100134. https://doi.org/10.1016/j.hazadv.2022.100134

[29] Shahbeik,H. Peng, W., Panahi, H., Dehhaghi, M., Guillemin, G., Fallahi, A., Amiri, H., Rehan, M., Raikwar, D., Latine, H., Pandalone, B., Khoshnevisan, B., Sonne, C., Vaccaro, L., Nizami, A., Gupta, V., Lam, S., Pan, J., Luque, R., Sels, B., Tabatabaei, M., Aghbashlo, M., 2022. Synthesis of liquid biofuels from biomass by hydrothermal gasification: A critical review. Renewable and Sustainable Energy Reviews. Volume 167. 112833. https://doi.org/10.1016/j.rser.2022.112833

[30] Shen, Y., 2020. A review on hydrothermal carbonization of biomass and plastic wastes to energy products. Biomass and Bioenergy. Volume 134. 105479. https://doi.org/10.1016/j.biombioe.2020.105479

[31] Amalina,F., Razak, A., Krishnan, S., Sulaiman, H., Zularisam, A., Nasrullah, M., 2022. A comprehensive assessment of the method for producing biochar, its characterization, stability, and potential applications in regenerative economic sustainability – A review. Cleaner Materials. Volume 3. 100045.

[32] Raval, N., Maheshwari, R., Kalyane, D., Ortiz, S., Chougule, M., Tekade, R., 2019. Chapter 10 - Importance of Physicochemical Characterization of Nanoparticles in Pharmaceutical Product Development. Basic Fundamentals of Drug Delivery. Pages 369-400. https://doi.org/10.1016/B978-0-12-817909-3.00010-8

[33] DeTata, D., Fillingham, R., D'Uva, J., 2023. Explosives: Overview. Encyclopedia of Forensic Sciences, Third Edition (Third Edition). Pages 356-390. https://doi.org/10.1016/B978-0-12-823677-2.00143-4

[34] Anderson, J., Voskerician, G., 2010. 14 - The challenge of biocompatibility evaluation of biocomposites. Biomedical Composites. Pages 325-353. https://doi.org/10.1533/9781845697372.3.325

[35] Holder, C., Schaak, R., 2019. Tutorial on Powder X-ray Diffraction for Characterizing Nanoscale Materials. American Chemical Society. Volume 13. Issue 7. Pages 7359-7365. https://doi.org/10.1021/acsnano.9b05157

[36] Bergström, J., 2015. 2 - Experimental Characterization Techniques. Mechanics of Solid Polymers. Pages 19-114.

[37] Basu, P., 2018. Chapter 14 - Analytical Techniques. Biomass Gasification, Pyrolysis and Torrefaction (Third Edition). Pages 479-495. https://doi.org/10.1016/B978-0-12-812992-0.00023-6

[38] Singh, M., Singh, A., 2022. Chapter 10 - Thermogravimetric analyzer. Characterization of Polymers and Fibres. Pages 223-240. https://doi.org/10.1016/B978-0-12-823986-5.00015-4

[39] Shi, X., Chen, Z., 2023. 12 - Characterizations of thermoelectric ceramics. Advanced Ceramics for Energy Storage, Thermoelectrics and Photonics. Pages 305-326. https://doi.org/10.1016/B978-0-323-90761-3.00002-4

[40] Sharma, R., Jasrotia, K., Singh, N., Ghosh, P., Srivastava, S., Sharma, N., Singh, J., Kanwar, R., Kumar, A., 2020. A Comprehensive Review on Hydrothermal Carbonization of Biomass and its Applications. Chemistry África. Volume 3. Pages 1-19. https://doi.org/10.1007/s42250-019-00098-3

[41] Islam, M., Limon, M., Romić, M., 2021. Hydrochar-based soil amendments for agriculture: a review of recent progress. Arabian Journal of Geosciences. Volume 14. 102. https://doi.org/10.1007/s12517-020-06358-8

[42] Han, L., Ro, K., Sun, K., Sun, H., Wang, Z., Libra, J., Xiang, B., 2016. New Evidence for High Sorption Capacity of Hydrochar for Hydrophobic Organic Pollutants. Environmental Science & Technology. Volume 50. Issue 24. https://doi.org/10.1021/acs.est.6b02401

[43] Islam, M., Sultana, A., Chambers, C., Saha, S., Saha, N., Kirtania, K., Reza, M., 2022. Recent Progress on Emerging Applications of Hydrochar. Energies. Volume 15. Issue 24. https://doi.org/10.3390/en15249340

[44] Fang, J., Zhan,L., Ok, Y., Gao, B., 2018. Minireview of potential applications of hydrochar derived from hydrothermal carbonization of biomass. Journal of Industrial and Engineering Chemistry. Volume 57. Pages 15-21. https://doi.org/10.1016/j.jiec.2017.08.026

[45] Ding, L., Wang, Z., Li, Y., Du, Y., Liu, H., Guo, Y., 2012. A novel hydrochar and nickel composite for the electrochemical supercapacitor electrode material. Materials Letters. Volume 74. Pages 111-114. https://doi.org/10.1016/j.matlet.2012.01.070

[46] Lin, Y., Ma, X., Peng, X., Hu, S., Yu, S., Fang, S., 2015. Effect of hydrothermal carbonization temperature on combustion behavior of hydrochar fuel from paper sludge. Applied Thermal Engineering. Volume 91. Pages 574-582. https://doi.org/10.1016/j.applthermaleng.2015.08.064

[47] Khan, Z., Javed, F., Shamair, Z., Hafeez, A., Fazal, T., Aslam, A., Zimmerman, W., Rehman, F., 2021. Current developments in esterification reaction: A review on process and parameters. Journal of Industrial and Engineering Chemistry. Volume 103. Pages 80-101. https://doi.org/10.1016/j.jiec.2021.07.018

[48] Almeida, E., Andrade, C., Santos, O., 2018. Production of Biodiesel Via Catalytic Processes: A Brief Review. International Journal of Chemical Reactor Engineering.Volume 16. Issue 5. DOI: 10.1515/ijcre-2017-0130

[49] Widayat, W., Wibowo, A., Hadiyanto, H., 2013. Study on Production Process of Biodiesel from Rubber Seed (Hevea Brasiliensis) by in Situ (Trans)Esterification Method with Acid Catalyst. Energy Procedia. Volume 32. Pages 64-73. Issue 64. DOI: 10.1016/j.egypro.2013.05.009

[50] Gebremariam, S., Marchetti, J., 2017. Biodiesel production tecnologies: Review. AIMS Energy. Volume 5. Pages 425-457. Issue 3. DOI:10.3934/energy.2017.3.425

[51] Dumesic, J., Huber, G., Boudart, M., 2008. Principles of Heterogeneous Catalysis. Handbook of Heterogeneous Catalysis. Volume 1. https://doi.org/10.1002/9783527610044.hetcat0001

[52] Klaewkla, R., Arend, M., Hölderich, W., 2011. A Review of Mass Transfer Controlling the Reaction Rate in Heterogeneous Catalytic Systems. Mass Transfer - Advanced Aspects. DOI:10.5772/22962

[53] Leeuwen, P., 2004. Homogeneous Catalysis. Understanding the Art. https://doi.org/10.1007/1-4020-2000-7

[54] Ribeiro, F., Santos, J., Araujo, R., Santos, V., Chaar, J., Tenório, J., Souza, K., 2024. Sustainable catalysts for esterification: Sulfonated carbon spheres from biomass waste using hydrothermal carbonization. Renewable Energy. Volume 220. 119653. https://doi.org/10.1016/j.renene.2023.119653

[55] Khethiwe, E., Clever K., Jekerias, G., 2020. Effects of Fatty Acids Composition on Fuel Properties of Jatropha Curcas Biodiesel. Smart Grid and Renewble Energy. Volume 11. DOI: 10.4236/sgre.2020.1110010

[56] Baishya, P., Mandal, M., Gogoi, P., Maji, T., 2017. Natural Polymer-Based Nanocomposites: A Greener Approach for the Future. Handbook of Composites from Renewable Materials. Pages 433-459. DOI:10.1002/9781119441632.ch139

[57] Knothe, G., 2005. Dependence of biodiesel fuel properties on the structure of fatty acid alkyl esters. Fuel Processing Technology. Volume 86. Pages 1059-1070. Issue 10. https://doi.org/10.1016/j.fuproc.2004.11.002

[58] Ockerman, H., Basu, L., 2024. By-products: Inedible. Encyclopedia of Meat Sciences (Third Edition). Pages 278-291. https://doi.org/10.1016/B978-0-323-85125-1.00052-1

[59] Foster, W., Azimov, U., Maradei, P., Molano, L., Combrinck, M., Munoz, J., Esteves, J., Patino, L., 2021. Waste-to-energy conversion technologies in the UK: Processes and barriers – A review. Renewable and Sustainable Energy Reviews. Volume 135. 110226.

[60] Hossain, N., Siddiqui, M., Balocch, H., Sabzoi, N., Mujawar, M., Mazari, S., Takkalkar, P., Abro, R., Sabzoi, A., Jatoi, A., 2020. Application of microwave synthesis in biodiesel production. Green Sustainable Process for Chemical and Environmental Engineering and Science Microwaves in Organic Synthesis. Pages 623-641. DOI:10.1016/B978-0-12-819848-3.00014-1

[61] Popovic, N., Wilson E., McQueen, C., 2017. Comprehensive Toxicology (Third Edition). Elsevier.

[62] Silva, M., Hori, C., Reis, M., 2015. Thermochemical data of the oleic acid esterification reaction: A quantum mechanics approach. Fluid Phase Equilibria. Volume 40. Pages 168-174. https://doi.org/10.1016/j.fluid.2015.07.050

[63] Romano, S., Sorichetti,P., 2010. Introduction to Biodiesel Production. Dielectric Spectroscopy in Biodiesel Production and Characterization. Pages 7-27. DOI: 10.1007/978-1-84996-519-4_2

[64] Atadashi,M. 2016. The effects of alcohol to oil molar ratios and the type of alcohol on biodiesel production using transesterification process. Egyptian Journal of Petroleum. Volume 25. Issue 1. DOI: 10.1016/j.ejpe.2015.06.007

[65] Erdiwansyay., Mamat, R., Sani, M., Sudhakar,K., Kadarohman,A. Sardjono, R., 2019. An overview of Higher alcohol and biodiesel as alternative fuels in engines.Energy Reports. Volume 5. Pages 467-479. https://doi.org/10.1016/j.egyr.2019.04.009

[66] Silva, M., Hori, C., Reis, M., 2015. Thermochemical data of the oleic acid esterification reaction: A quantum mechanics approach. Fluid Phase Equilibria. Volume 406. Pages 168-174. https://doi.org/10.1016/j.fluid.2015.07.050

[67] Gupta, V., Singh, K., 2023. The impact of heterogeneous catalyst on biodiesel production; a review. Materials Today: Proceedings. Volume 78. Part 3. Pages 364-371. https://doi.org/10.1016/j.matpr.2022.10.175

[68] Khalid, A., 2021. Synthesis of Iron Molybdate and Evaluation of the Methods (Review). International Journal of Innovative Research in Science Engineering and Technology. Volume 6. Pages 548-593. Issue 1.

[69] Fattah, I., Ong, H., Mahlia, T., Mofijur, M., Silitonga, A., Rahman, S., Ahmad, A., 2020. State of the Art of Catalysts for Biodiesel Production. Frontiers in Energy Research. Volume 8. DOI:10.3389/fenrg.2020.00101

[70] Talha, N., Sulaiman, S., 2016. Overview Of Catalysts In Biodiesel Production. ARPN Journal of Engineering and Applied Sciences. Volume 11. Issue 1.

[71] Nawaz, S., Ahmad, M., Asif, S., Klemeš, J., Mubashir, M., Munir, M., Zafar, M., Bokhari, A., Mukhtar, A., Saqib, S., Khoo, K., Show, P., 2022. Phyllosilicate derived catalysts for efficient conversion of lignocellulosic derived biomass to biodiesel: A review. Bioresource Technology. Volume 343. 126068. https://doi.org/10.1016/j.biortech.2021.126068

[72] Borugadda, V., Goud, V., 2012. Biodiesel production from renewable feedstocks: Status and opportunities. Renewable and Sustainable Energy Reviews. Volume 16. Pages 4763-4784. Issue 7. https://doi.org/10.1016/j.rser.2012.04.010

[73] Maheshwari, P., Haider, M., Yusuf, M., Klemeš, J., Bokhari, A., Beg, M., Othman, A., Kumar, R., Jaiswal, A., 2022. A review on latest trends in cleaner biodiesel production: Role of feedstock, production methods, and catalysts. Journal of Cleaner Production. Volume 355. 131588. https://doi.org/10.1016/j.jclepro.2022.131588

[74] Chorkendorff, I., Niemantsverdriet,J., 2003. Concepts of Modern Catalysis and Kinetics. Wiley-VCH Verlag GmbH & Co. KGaA. DOI:10.1002/3527602658.

[75] Campbell, I., 1988. Catalysis at surfaces. Chapman and Hall. 17548725.

[76] Yan, Y., Li, X., Wang, G., Gui, X., Li, G., Su, F., Wang, X., Liu, T., 2014. Biotechnological preparation of biodiesel and its high-valued derivatives: A review. Applied Energy. Volume 113. Pages 1614-1631. https://doi.org/10.1016/j.apenergy.2013.09.029

[77] Changmai, B., Vanlalveni, C., Ingle, A., Bhagat, R., Rokhum, S.,2020. Widely used catalysts in biodiesel production: a review. RSC Advances. Volme 10. Pages 41625-41679. Issue 68. https://doi.org/10.1039/D0RA07931F

[78] Dias, A., Catarino, M., Gomes, J., 2021. Co-processing lard/soybean oil over Ca-based catalysts to greener biodiesel. Environmental Technology & Innovation. Volume 21. 101220. https://doi.org/10.1016/j.eti.2020.101220

[79] Su, F., Guo, Y., 2014. Advancements in solid acid catalysts for biodiesel production. Green Chemistry. Volume 16. Pages 2934-2957. Issue 6. https://doi.org/10.1039/C3GC42333F

[80] Ramos, M., Dias, A., Puna, J., Gomes, J., Bordado, J., 2019. Biodiesel Production Processes and Sustainable Raw Materials. Energies. Volume12. Issue 23. https://doi.org/10.3390/en12234408

[81] Zheng, F., Cho, H., 2024. The Effect of Different Mixing Proportions and Different Operating Conditions of Biodiesel Blended Fuel on Emissions and Performance of Compression Ignition Engines. Energies. Volume 17. Issue 2. https://doi.org/10.3390/en17020344

[82] European Biodiesel Board. About Biodiesel. https://ebb-eu.org/about-biodiesel-2/ - Accessed 5 Jully 2024.

[83] Nabgan, W., Jalil, A., Nabgan, B., Jadhav, A., Ikram, M., Hamid, A., Ali, M., Sahida, N., 2022. Sustainable biodiesel generation through catalytic transesterification of waste sources: a literature review and bibliometric survey. RSC Advances. Volume 12. Pages 1604-1627. Issue 3. https://doi.org/10.1039/D1RA07338A

[84] Akram, F., Haq, I., Raja, S., Mir, A., Qureshi, S., Aqeel, A., Shah, F., 2022. Current trends in biodiesel production technologies and future progressions: A possible displacement of the petro-diesel. Journal of Cleaner Production. Volume 370. 133479. https://doi.org/10.1016/j.jclepro.2022.133479

[85] Shukla, S., Rathore, P., 2020. Chapter 14 - Production of biodiesel and its application in engines. Waste Biorefinery. Pages 379-389. https://doi.org/10.1016/B978-0-12-818228-4.00014-9

[86] Ogunkunle, O., Ahmed, N., 2019. A review of global current scenario of biodiesel adoption and combustion in vehicular diesel engines. Energy Reports. Volume 5. Pages 1560-1579. https://doi.org/10.1016/j.egyr.2019.10.028

[87] Silva, K., Corazza, M., Jr, J., 2018. Renewable Energy Sources: A Sustainable Strategy for Biodiesel Productions. Increased Biodiesel Efficiency. Pages 1-31. https://doi.org/10.1007/978-3-319-73552-8_1

[88] Ghobadian, B., Rahimi, H., Nikbakht, A., Najafi, G., Yusaf, T., 2009. Diesel engine performance and exhaust emission analysis using waste cooking biodiesel fuel with an artificial neural network. Renewable Energy. Volume 34. Pages 976-982. Issue 4. https://doi.org/10.1016/j.renene.2008.08.008

[89] Enweremadu, C., Peleowo, A., Rutto, H., 2011. Performance evaluation of a diesel engine fueled with methyl ester of shea butter. World Academy of Science, Engineering and Technology. Volume 7. Issue 79. https://doi.org/10.5281/zenodo.1327857

[90] Liu, Y., Jr, J., 2006. Effect of carbon chain length on esterification of carboxylic acids with methanol using acid catalysis. Journal of Catalysis. Volume 243. Pages 221-228. Issue 2. https://doi.org/10.1016/j.jcat.2006.07.013

[91] Liu, Y., Lotero, E., Jr, J., 2006. Effect of water on sulfuric acid catalyzed esterification. Journal of Molecular Catalysis A: Chemical. Volume 245. Pages 132-140. Issues 1-2. https://doi.org/10.1016/j.molcata.2005.09.049

[92] Dias, A., Saraiva, N., Rijo, B., Pereira, M., Santos, L., Galhano, R., Paulo, I., 2024. Sugar derived hydrochar catalysts for enhanced biodiesel production via esterification. Fuel. Volume 374. 132459. https://doi.org/10.1016/j.fuel.2024.132459

[93] Yadav, N., Yadav, G., Ahmaruzzaman, M., 2023. Biomass-derived sulfonated polycyclic aromatic carbon catalysts for biodiesel production by esterification reaction. Biofuels, Bioproducts and Biorefining. Volume 17. Pages 1343-1367. Issue 5. https://doi.org/10.1002/bbb.2486

[94] Kilani, A., Olubambi, A., Ikotun, B., Adeleke, O., 2022. Structural Performance of Concrete Reinforced with Banana and Orange Peel Fibers -A Review. Journal of Sustainable Construction Materials and Technologies. Volume 7. Issue 4. DOI:10.47481/jscmt.1144427

[95] Khan, M., Perveen, B., 2010. Transformation of Agricultural Wastes into Sugar by Trichoderma viride. Journal of Pure and Applied Microbiology. Volume 4. Pages 103-108. Issue 1.

[96] Yaashikaa, P., Kumar, P., Varjani, S., Saravanan, A., 2020. A critical review on the biochar production techniques, characterization, stability and applications for circular bioeconomy. Biotechnology Reports. Volume 28. e00570. https://doi.org/10.1016/j.btre.2020.e00570

[97] Chaves, P., Cepeda, J., Álvarez, F., Orzáez, M., 2020. Influence of Moisture, Temperature and Microbial Activity in Biomass Sustainable Storage. Special Focus on Olive Biomasses. International Journal of Environmental Sciences & Natural Resources. Volume 25. Issue 3. Doi: 10.19080/IJESNR.2020.25.556165

[98] Saha, N., Hernandez, S., Jin, W., Westover,T., Klinger, J., 2022. Characterization of particle size and moisture content effects on mechanical and feeding behavior of milled corn (Zea mays L.) stover. Powder Technology. Volume 45. 117535. https://doi.org/10.1016/j.powtec.2022.117535

[99] Petrović, j., Ercegović, M., Simić, M., Koprivica, M., Dimitrijević, J., Jovanović, A., Pantić, J., 2024. Hydrothermal Carbonization of Waste Biomass: A Review of Hydrochar Preparation and Environmental Application. Processes. Volume 12. Issue 1. https://doi.org/10.3390/pr12010207

[100] Plavniece, A., Dobele, G., Volperts, A., Zhurinsh, A., 2022. Hydrothermal Carbonization vs. Pyrolysis: Effect on the Porosity of the Activated Carbon Materials. Sustainability. Volume 14. Issue 23. https://doi.org/10.3390/su142315982

[101] Khoshbouy, R., Leijiu, R., Takahashi, F., Yoshikawa, K., 2018. Effect of acid-assisted hydrothermal carbonization (HTC) process of tree branches using nitric acid on cadmium adsorption. E3S Web of Conferences. Volume 67. https://doi.org/10.1051/e3sconf/20186703033

[102] Kovalenko, H., Moser, K., Warzala, M., Holzer, A., Stańczyk, D., Sabura, E., 2021. Selected Fatty Acids Esters as Potential PHB-V Bioplasticizers: Effect on Mechanical Properties of the Polymer. Journal of Polymers and the Environment. Volume 29. Issue 11. DOI:10.1007/s10924-020-01841-5

[103] Yang, K., Peng, H Wen, Y., Li, N., 2010. Re-examination of characteristic FTIR spectrum of secondary layer in bilayer oleic acid-coated Fe3O4 nanoparticles. Applied Surface Science. Volume 256. Pages 3093-3097. Issue 10. https://doi.org/10.1016/j.apsusc.2009.11.079

[104] Mafra, M., Mafra, L., Zuim, D., Vasques, É., Ferreira, M., 2013. Adsorption Of Remazol Brilliant Blue on Na Orange Peel Adsorbent. Brazilian Journal of Chemical Engineering. Volume 30. Pages 657-665. DOI:10.1590/S0104-66322013000300022

[105] Kazak, O., Tor, A., 2020. In situ preparation of magnetic hydrochar by co-hydrothermal treatment of waste vinasse with red mud and its adsorption property for Pb(II) in aqueous solution. Journal of Hazardous Materials Advances. Volume 393. https://doi.org/10.1016/j.jhazmat.2020.122391

[106] Vimal, V., Karim, A., Kumar, M., Ray, A., Biswas, K., Maurya, S., Subudhi, D., Dhal, N., 2022. Nutrients enriched biochar production through Co-Pyrolysis of poultry litter with banana peduncle and phosphogypsum waste. Chemosphere. Volume 300. 134512. https://doi.org/10.1016/j.chemosphere.2022.134512.

[107] Oyeyinka, B., Afolayan, A., 2019. Comparative Evaluation of the Nutritive. Mineral, and Antinutritive Composition of Musa sinensis L. (Banana) and Musa paradisiaca L. (Plantain) Fruit Compartments. Plants (Basel). Volume 8. Issue 12. DOI:10.3390/plants8120598

[108] Bratovcic, A., 2020. Effect of Temperature Extraction on the Potassium and Calcium Content in the Lemon and Orange Water Peel Exxtracts. Journal Of Advances In Chemistry. Volume 17. Pages 35-43. Issue 1. DOI:10.24297/jac.v17i.8714

[109] Ghahramanifard, F., Rouhollahi, A., Fazlolahzadeh, O., 2018. Electrodeposition of Cu-doped p-type ZnO nanorods; effect of Cu doping on structural, optical and photoelectrocatalytic property of ZnO nanostructure. Superlattices and Microstructures. Volume 114.Pages 1-14. https://doi.org/10.1016/j.spmi.2017.07.019.

[110] Tighsazzadeh, D., Mitchell, J., Boateng, J., 2019. Development and evaluation of performance characteristics of timolol-loaded composite ocular films as potential delivery platform for treatment of glaucoma. International Journal of Pharmaceutics. Volume 566. Issue 1. Doi: 10.1016/j.ijpharm.2019.05.059.

[111] Boyle, R., Sukumaran, S., Chen, R., Quantitative determination of hydrogen concentration in silicon nitride dielectric films on silicon wafers using FTIR spectroscopy. ThermoFisher Scientific. 2022. https://assets.thermofisher.com/TFS-Assets%2FMSD%2FApplication-Notes%2FAN53081-quantitative-determination-hydrogen-SiN-wafers-ftir.pdf

[112] Elsaid, S., Anwar, N., Roushdi, M., 2024. Pesticides' low-cost removal from polluted groundwater using charcoal from "Salix mucronata" trees activated by gold nitrate. Water Science. Volume 38. Pages 48-64. Doi:10.1080/23570008.2023.2290764.

[113] Rozali, M., Ahmad, N., Isa, M., Nizam, I., 2015. Effect of Adipic Acid Composition on Structural and Conductivity Solid Biopolymer Electrolytes Based on Carboxy Methylcellulose Studies. American-Eurasian Journal of Sustainable Agriculture. Volume 9. Pages 39-45. Issue 2.

[114] Spataru, D., Dias, A., Ferreira, L., 2021. Acetylation of biodiesel glycerin using glycerin and glucose derived catalysts. Journal of Cleaner Production. Volume 297. 126686. https://doi.org/10.1016/j.jclepro.2021.126686

[115] Khosroshahi, A., Dizaj, S., Sharifi, S., Torab, A., Negahdari, R., Aghbolaghi, N., Vahedi, P., 2022. The Preparation, the Physicochemical Assessment, and the Antimicrobial Action of Nanocurcumin-Loaded Dental Temporary Restorative Material. Journal of Nanomaterials. Pages 1-7. Doi:10.1155/2022/5339809.

[116] Egbuonu, A., Amadi, C., 2016. Some Nutritive and Antifungal Properties of Citrus sinensis (Sweet Orange) Peels and Seeds. American Chemical Science Journal. Volume 14. Pages 1-7. Doi:10.9734/ACSJ/2016/25647.

[117] Khalil, K., Ahmed, H., Bashal, A., Bräse, S., Nayl, A., Gomha, S., 2022. Efficient, Recyclable, and Heterogeneous Base Nanocatalyst for Thiazoles with a Chitosan-Capped Calcium Oxide Nanocomposite. Polymers. Volume 14. 3347. Doi:10.3390/polym14163347.

[118] Kang, S., Lee, K., Singh, M., Vinayagam, R., 2023. Salicylic-Zinc Nanocomposites with Enhanced Antibacterial Activity. Coatings. Volume 13. Issue 5. 941. Doi:10.3390/coatings13050941.

[119] Hien, N., Jones, E., Vinh, N., Phu, T., Tam, N., Lynch, I., 2018. Physicochemical Characterization of Biomass Residue-Derived Biochars in Vietnam. Doi:10.20944/preprints201807. 0403.v1.

[120] Nishshankage, K., Wijerathna, C., Ezzat, A., Zhang, X., Vithanage, Me., 2023. Antifungal efficacy of biogenic waste derived colloidal/nanobiochar against Colletotrichum gloeosporioides species complex. Environmental research. Volume 241. 117621. 10.1016/j.envres.2023.117621.

[121] Nájar, N., Hurtado, J., Ramos, E., Pulido, G., Ibarra, A., Espadas, A., 2023. Magnetic Biochar Obtained by Chemical Coprecipitation and Pyrolysis of Corn Cob Residues: Characterization and Methylene Blue Adsorption. Materials. Volume 16. 3127. Doi:10.3390/ma16083127.

[122] Park, J., Ok, Y., Kim, S., Kang, S., Cho, J., Heo, J., Delaune, R., Seo, D., 2015. Characteristics of biochars derived from fruit tree pruning wastes and their effects on lead adsorption. Journal of the Korean Society for Applied Biological Chemistry. Volume 58. Pages 751–760. https://doi.org/10.1007/s13765-015-0103-1

[123] Zhang, M., Liu, Y., Yin, Z., Feng, D., Lv, Hui., 2023. Preparation and adsorption properties of magnetic chitosan/sludge biochar composites for removal of Cu ions. Scientific Reports. Volume 13. Doi:10.1038/s41598-023-46815-4.

[124] Salim, R., Asik, J., Sarjadi, M., 2021. Chemical functional groups of extractives, cellulose and lignin extracted from native Leucaena leucocephala bark. Wood Science and Technology. Volume 55. Pages 295-313. https://doi.org/10.1007/s00226-020-01258-2.

[125] Liu, S., Peng, S., Zhang, B., Xue, B., Yang, Z., Wang, S., Xu, G., 2022. Effects of biochar pyrolysis temperature on thermal properties of polyethylene glycol/biochar composites as shape-stable biocomposite phase change materials. RSC Advances. Volume 12. Pages 9587-9598. Doi: 10.1039/D1RA09167K.

[126] Marrocchi, A., Cerza, E., Chandrasekaran, S., Sgreccia, E., 2024. Hydrochar from Pine Needles as a Green Alternative for Catalytic Electrodes in Energy Applications. Volume 29. Issue 14. Doi:10.3390/molecules29143286.

[127] Kumar, A., Choudhary, R., Narzari, R., Kataki, R., Shukla, S. K., Chailleux, E., 2018. Evaluation of bio-asphalt binders modified with biochar: a pyrolysis by-product of Mesua ferrea seed cover waste. Cogent Engineering. Volume 5. https://doi.org/10.1080/23311916.2018.1548531284

[128] Ilić, M., Haegel, F., Lolić, A., 2022. Surface functional groups and degree of carbonization of selected chars from different processes and feedstock. PLoS One. Volume 17. Issue 11. Doi: 10.1371/journal.pone.0277365

[129] Schnitzer, M., Monreal, C., Facey, G., Fransham, P., 2007. The conversion of chicken manure to biooil by fast pyrolysis I. Analyses of chicken manure, biooils and char by 13 C and 1 H NMR and FTIR spectrophotometry. Journal of environmental science and health. Part. B, Pesticides, food contaminants, and agricultural wastes. Volume 42. Pages 71-7. Doi:10.1080/03601230601020894

[130] Patkowska, S., Madej, J., 2018. Comparison of photoacoustic, diffuse refl ectance, attenuated total reflectance and transmission infrared spectroscopy for the study of biochars. Polish Journal of Chemical Technology. Volume 20. Issue 4. Pages 75-83. Doi:10.2478/pjct-2018-0057.

[131] Pusceddu. E., 2017. Comparison between ancient and fresh biochar samples, a study on the recalcitrance of carbonaceous structures during soil incubation. International Journal of New Technology and Research. Volume 3. Issue 3. Pages 39-46.

[132] Zhang, S., Min, Z., Tay, H., Asadullah, M., Li, C., 2011. Effects of volatile-char interactions on the evolution of char structure during the gasification of Victorian brown coal in steam. Fuel. Volume 90. Pages 1529-1535. Issue 4. https://doi.org/10.1016/j.fuel.2010.11.010

[133] Cao, B., Yuan, J., Jiang, D., Wang, S., Barati, B., Hu, Y., Yuan, C., Gong, X., Wang, Q., 2021. Seaweed-derived biochar with multiple active sites as a heterogeneous catalyst for converting macroalgae into acid-free biooil containing abundant ester and sugar substances. Fuel. Volume 285. 119164. https://doi.org/10.1016/j.fuel.2020.119164

[134] Wang, C., Xie, Q., Dou, X. et al., 2023. Conversion of carbonaceous materials into solid acids for tylosin mitigation: effect of preprocessing methods on the reactivity of sulfonation reaction. Biochar. Volume 5 https://doi.org/10.1007/s42773-023-00230-0

[135] Gu, W., Sevilla, M., Magasinki, A., Fuertes, A., Yushin, G., 2013. Sulfur-containing activated carbons with greatly reduced content of bottle neck pores for double-layer capacitors: a case study for pseudocapacitance detection. Energy & Environmental Science. Volume 6. Pages 2465-2476. Issue 8. https://doi.org/10.1039/C3EE41182F

[136] Corrêa, A., Silva, P., Gonçalves,M., Bastos, R., Filho, G., Conceição, L., 2023. Study of the activity and stability of sulfonated carbon catalyst from agroindustrial waste in biodiesel production: Influence of pyrolysis temperature on functionalization. Arabian Journal of Chemistry. Volume 16. Issue 8. https://doi.org/10.1016/j.arabjc.2023.104964

[137] Gagić, T., Uzunalić, A., Knez, Ž., Škerget, M., 2018. Hydrothermal Degradation of Cellulose at Temperature from 200 to 300°C. Industrial & Engineering Chemistry Research. Volume 57. Pages 6576-6584. Issue 18. https://doi.org/10.1021/acs.iecr.8b00332

[138] Wortmann, M., Keil, W., Brockhagen, B., Biedinger, J., Westphal, M., Weinberger, C., Diestelhorst, E., Hachmann, W., Zhao, Y., Tiemann, M., Reiss, G., et all., 2022. Pyrolysis of sucrose-derived hydrochar. Journal of Analytical and Applied Pyrolysis. Volume 161. 105404. https://doi.org/10.1016/j.jaap.2021.105404

[139] Welles, T., Ahn, J., 2021. Driving electrochemical corrosion of implanted CoCrMo metal via oscillatory electric fields without mechanical wear. Scientific Reports. Volume 11. Doi:10.1038/s41598-021-01810-5

[140] Enein, A., Salama, Z., Gaafar, A., Aly,H., Elella, F.,Ahmed, H., 2016. Identification of phenolic compounds from banana peel (Musa paradaisica L.) as antioxidant and antimicrobial agents. Journal of Chemical and Pharmaceutical Research. Issue 46. Pages 46-55.

[141] Hasanah, A., Rizkiana, F., Rahayu, D., 2012. Banana Peels And Stem (Musa x paradisiaca Linn.) As Biosorbent Of Copper In Textile Industry Wastewater. Research Journal of Pharmaceutical, Biological and Chemical Sciences. Volume 3 Issue 3. Pages 1171-1178. ISSN: 0975-8585